# Copepod life strategy and population viability in response to prey timing and temperature: Testing a new model across latitude, time, and the size spectrum

**Neil S. Banas** [1,*], **Eva Friis Møller** [2], **Torkel Gissel Nielsen** [3], **and Lisa B. Eisner** [4]

[1] *Department of Mathematics and Statistics, University of Strathclyde, Glasgow, UK*
[2] *Department of Bioscience, Aarhus University, Roskilde, Denmark*
[3] *National Institute of Aquatic Resources, Section for Ocean Ecology and Climate, Technical University of Denmark, Charlottenlund, Denmark*
[4] *NOAA Fisheries, Alaska Marine Science Center, Seattle, Washington, USA*

Correspondence*:
Neil S. Banas
Dept. of Mathematics and Statistics, Univ. of Strathclyde, 26 Richmond St., Glasgow G1 1XQ, UK, neil.banas@strath.ac.uk

## ABSTRACT

A new model (”Coltrane”: Copepod Life-history Traits and Adaptation to Novel Environments) describes environmental controls on copepod populations via 1) phenology and life history and 2) temperature and energy budgets in a unified framework. A set of complementary model experiments are used to determine what patterns in copepod community composition and productivity can be predicted from only a few key constraints on the individual energy budget: the total energy available in a given environment per year; the energy and time required to build an adult body; the metabolic and predation penalties for taking too long to reproduce; and the size and temperature dependence of the vital rates involved. In an idealized global-scale testbed, the model correctly predicts life strategies in large *Calanus* spp. ranging from multiple generations per year to multiple years per generation. In a Bering Sea testbed, the model replicates the dramatic variability in the abundance of *C. glacialis/marshallae* observed between warm and cold years of the 2000s, and indicates that prey phenology linked to sea ice is a more important driver than temperature per se. In a Disko Bay, West Greenland testbed, the model predicts the viability of a spectrum of large-copepod strategies from income breeders with a adult size $\sim$ 100 $\mu$gC reproducing once per year through capital breeders with an adult size $>$ 1000 $\mu$gC with a multiple-year life cycle. This spectrum corresponds closely to the observed life histories and physiology of local populations of *C. finmarchicus*, *C. glacialis*, and *C. hyperboreus*.

**Keywords: Zooplankton, copepod, life history, annual routine, diversity, biogeography, modelling, community ecology, Arctic**

## 1 INTRODUCTION

Calanoid copepods occupy a crucial position in marine food chains, the dominant mesozooplankton in many temperate and polar systems, important to packaging of microbial production in a form accessible to higher predators. They also represent the point at which biogeochemical processes, and numerical approaches like NPZ (nutrient–phytoplankton–zooplankton) models, start to be significantly modulated by life-history and behavioural constraints. The population- and community-level response of copepods to environmental change (temperature, prey availability, seasonality) thus forms a crucial filter lying between the biogeochemical impacts of climate change on primary production patterns and the food-web impacts that follow.

Across many scales in many systems, the response of fish, seabirds, and marine mammals to climate change has been observed, or hypothesized, to follow copepod community composition more closely than it follows total copepod or total zooplankton production. Examples include interannual variation in pollock recruitment in the Eastern Bering Sea (Coyle et al., 2011; Eisner et al., 2014), interdecadal fluctuations in salmon marine survival across the Northeast Pacific (Mantua et al., 1997; Hooff and Peterson, 2006; Burke et al., 2013), and long-term trends in forage fish and seabird abundance in the North Sea (Beaugrand and Kirby, 2010; MacDonald et al., 2015). These cases can be all be schematized as following the "junk food" hypothesis (Österblom et al., 2008) in which the crucial axis of variation is not between high and low total prey productivity, but rather between high and low relative abundance of large, lipid-rich prey taxa.

Calanoid copepods range in adult body size by more than two orders of magnitude, from $<10$ to $>1000$ $\mu$g C. Lipid storage is likewise quite variable among species, and linked to both overwintering and reproductive strategy (Kattner and Hagen, 2009; Falk-Petersen et al., 2009). Many but not all species enter a seasonal period of diapause in deep water, in which they do not feed and basal metabolism is reduced to $\sim$1/4 of what it is during active periods (Maps et al., 2014). Reproductive strategies include both income breeding (egg production fueled by ingestion of fresh prey during phytoplankton blooms) and capital breeding (egg production fueled by stored lipids in winter), as well as hybrids between the two strategies (Hirche and Kattner, 1993; Daase et al., 2013). Generation lengths vary from several weeks to several years.

This paper describes a numerical approach, appropriate for both regional and global scales, that predicts many of these traits—adult size, average lipid/energy content, life cycle, and seasonal timing—from first principles based on interactions among growth, development, reproduction, and survivorship. Our approach draws on two currents in recent modelling work. First, it builds on the *optimal annual routine* approach (McNamara and Houston, 2008) previously applied to copepods by Varpe et al. (2007, 2009) and others. We borrow from this tradition the hypothesis, or instinct, that timing is everything in seasonal environments, as well as the technical strategy of separately tracking structural and reserve energy stores, with the latter variable forming a link between copepod survival strategy and the value of the copepods as prey. Second, we embed this optimal-annual-routine logic in a *trait-based metacommunity* (Follows et al., 2007; Record et al., 2013), in which a small number of traits is used to parsimoniously represent the possibility space of "all ways there are to be a copepod."

The model experiments below pose the question: How many of the high-level associations among copepod body size, body composition, generation length, reproductive strategy, and annual routine, at global or regional scales, can be explained by a small handful of traits and tradeoffs that regulate how individual animals best allocate energy over time? We will show that the scheme introduced here reproduces patterns in space (large-scale trait biogeography), time (variability of one *Calanus* sp. in the Bering Sea), and along

the size spectrum (differences among three coexisting *Calanus* spp. in Disko Bay, West Greenland), in response to annual cycles of temperature and prey availability.

## 2 MODEL DESCRIPTION

### 2.1 General approach

The model introduced here is "Coltrane" (Copepod Life-history Traits and Adaptation to New Environments) version 1.0. Like many individual-based models Fiksen and Carlotti (1998), Coltrane represents the time-evolution of one cohort of a clonal population, all bearing the same traits and spawned on the same date $t_0$, with a set of ODEs. The state variables describing a cohort are relative developmental stage $D$, where $D = 0$ represents a newly spawned egg and $D = 1$ an adult; survivorship $N$, the fraction of initially spawned individuals that remain after some amount of cumulative predation mortality; activity level $a$, 1 for normal activity and 0 for diapause; structural biomass per individual $S$, and "potential" or "free scope" $\varphi$, which represents all net energy gain not committed to structure, i.e. a combination of internal energy reserves and eggs already produced. Combining reserves and eggs into one pool in this way lets us cleanly separate results that depend only on the fundamental energy budget (gain from ingestion, loss to metabolism, and energy required to build somatic structure) from results that depend on particular assumptions about egg production (costs, cues, and strategies). An alternate form of the model explicitly divides $\varphi$ into internal reserves $R$ and income and capital egg production rates $E_{inc}$ and $E_{cap}$: the simpler model without this distinction will be called the "potential" or $\varphi$ model and the fuller version the "egg/reserve" or ER model.

Because our goal is to describe a broad landscape of potentially coexisting strategies rather than a single, optimal strategy, the model is written as a family of parallel, forward-in-time integrations with traits varying among cases, rather than using the backwards-in-time solving method of the classic optimal annual routine approach (Houston et al., 1993; Varpe et al., 2007). The model uses a family of cases varying spawning date $t_0$ over the year to produce population-level results, and families of cases varying one or more traits to produce community-level results.

In contrast to Record et al. (2013), we do not include interactions between competing species or explicitly resolve coexistence and its limits, keeping our representation of predation mortality simple and linear to make this possible. The purpose of this simplification (beyond a huge increase in computational efficiency) is to separate bottom-up from top-down mechanisms as fully as possible, for the sake of interpretability. Record et al. (2013) show that the choice of mortality closure has a huge effect on predictions of community structure and diversity, and this dependence can easily obscure one's understanding of how temperature and prey cycles affect community characteristics by themselves.

Because we are willfully ignoring competition and coupling through predation, we will evaluate model results in terms of the *landscape of viable strategies in a given environment*, rather than treating the results as detailed predictions of relative abundance. A particular environment is defined by annual cycles of three variables, total concentration of phytoplankton/microzooplankton prey $P$, surface temperature $T_0$, and deep temperature $T_d$. At present, these annual cycles are assumed to be perfectly repeatable, so that a "viable" strategy can be defined as a set of traits that lead to annual egg production above the replacement rate, given $P$, $T_0$, and $T_d$ as functions of yearday $t$. The effect of interannual variability on strategy is left for future work.

## 2.2 Time evolution of one cohort

### 2.2.1 Ontogenetic development

Calanoid copepods have a determinate developmental sequence, comprising the embryonic period, six naupliiar stages (N1–6), five copepodid stages (C1–5) and adulthood (C6). Similar to Maps et al. (2012), conversions between relative developmental stage $D$ and the actual 13-stage sequence have been done using relative stage durations for *C. finmarchicus* from (Campbell et al., 2001), which appear to be appropriate for other *Calanus* spp. with the proviso that C5 duration is particularly variable and strategy-dependent. Development in the model follows

$$\frac{dD}{dt} = u, \quad D \leq 1 \tag{1}$$

where developmental rate $u$ is

$$u = a\, q_d\, \sigma\, u_0 \tag{2}$$

and

$$q_d \equiv Q_d^{T/10^\circ\mathrm{C}} \tag{3}$$

$$T = a\, T_0 + (1-a)\, T_d \tag{4}$$

$$\sigma \equiv \frac{P}{K_s + P} \tag{5}$$

All variables and parameters are defined in Table 1. The temperature-dependent factor $q_d$ describes a power-law response with a $Q_{10}$ of $Q_d$, where temperature is assumed to be $T_0$ during active feeding ($a = 1$) and $T_d$ during diapause ($a = 0$). Prey saturation $\sigma$ is a simple Michaelis-Menten function with half-saturation $K_s$. The parameter $u_0$, the development rate corrected to 0°C, was found by Banas and Campbell (2016) to be the primary trait responsible for differences in adult body size among *Calanus* spp. and other calanoids >50 $\mu$g C adult size, although not at a broader scale of diversity.

### 2.2.2 Energy gain and loss

Energy gain from ingestion is given by

$$I = a\, r_a\, \sigma\, q_g\, I_0\, S^{\theta-1} \tag{6}$$

Ingestion is assumed to follow a Kleiber's Law-like size dependence, with $\theta$ = 0.7 (Kleiber, 1932; Saiz and Calbet, 2007). $I_0$ is specific ingestion rate at saturating prey concentration, $T$=0°C, and $S$=1 $\mu$g C.

The factor $q_g \equiv Q_g^{T/10^\circ\mathrm{C}}$ is a power-law temperature response for growth parallel to that for development but with a different $Q_{10}$. $Q_{10}$ values have been found to vary among copepod species but Banas and Campbell (2016) argue that common values derived from a fit across community-level data are more appropriate for comparing species near their thermal optima. Based on Forster et al. (2011), we use $Q_g$ = 2.5 and $Q_d$ = 3.0.

Energy loss to metabolism is given by

$$M = a^\star\, r_m\, q_g\, I_0\, S^{\theta-1} \tag{7}$$

where $r_m$ is the ratio of metabolism to ingestion when prey is saturating. Unlike $dD/dt$ and $I$, which are 0 during diapause ($a = 0$: see below) because of the factor $a$ in (2) and (6), $M$ during diapause is nonzero,

although reduced by a factor $r_b$:

$$a^\star = r_b + (1 - r_b)a \tag{8}$$

In this formalism, gross growth efficiency $\epsilon$ can be written

$$\epsilon = \frac{I - M}{r_a^{-1} I} = \sigma r_a - r_m \tag{9}$$

We have set $r_m$ = 0.14 such that $\epsilon \approx 0.3$ when $P \approx 2K_s$ and $\epsilon = 0$ when $P = 1/4\ K_s$.

### 2.2.3 Allocation of net gain

Net mass-specific energy gain $G$ is simply $I - M$. The two energy stores $S$ and $\varphi$ follow

$$\frac{dS}{dt} = f_s G S \tag{10}$$

$$\frac{d\varphi}{dt} = (1 - f_s) G S \tag{11}$$

in the case where $G \geq 0$ and development is past the first feeding stage, $D \geq D_f$. For $D < D_f$, we assume $G = 0$ for simplicity. Positive gain is allocated between structure and potential according to the factor $f_s$, which commits net gain entirely to structure before a developmental point $D_s$, entirely to potential during adulthood, and to a combination of them in between:

$$f_s = \begin{cases} 1, & D < D_s \\ \frac{1-D}{1-D_s}, & D_s \leq D \leq 1 \\ 0, & D = 1 \end{cases} \tag{12}$$

When $G \leq 0$, the deficit is taken entirely from reserves (eq. (11) with $f_s$=0).

Potential $\varphi$ is allowed to run modestly negative, to represent consumption of body structure during starvation conditions. A cohort is terminated by starvation if

$$\varphi < -r_{starv} S \tag{13}$$

where in this study $r_{starv}$ = 0.1. A convenient numerical implementation of this scheme is to integrate $S$ implicitly so that it is guaranteed $> 0$, and to integrate $\varphi$ explicitly so that it is allowed to change sign, with no change of dynamics at $\varphi = 0$.

### 2.2.4 Reserves vs. potential reserves

If the $\varphi$ model just described is elaborated with an explicit scheme for calculating total egg production over time $E(t)$, then it is possible to define $R(t)$, individual storage/reserve biomass, and interpret $R$ as a state variable and $\varphi$ as a derived quantity. The relationship between the two is

$$\frac{dR}{dt} = (1 - f_s) G S - E \tag{14}$$

$$\varphi(t) = R(t) + \int_{t_0}^{t} E(t')\, dt' \tag{15}$$

Thus $\varphi$ tracks the reserves that an animal would have remaining if it had not previously started egg production. This is a useful metric for optimising reproductive timing, as we will show (Section 2.3).

### 2.2.5 Predation mortality

Predation mortality is assumed to have the same dependence on temperature and body size as ingestion, metabolism, and net gain (Hirst and Kiørboe, 2002). Survivorship $N$ is set to 1 initially and decreases according to

$$\frac{d(\ln N)}{dt} = -m \tag{16}$$

where

$$m = a\, q_g\, S^{\theta-1}\, m_0 \tag{17}$$

so that predation pressure relative to energy gain is encapsulated in a single parameter $m_0$. In practice $m_0$ is a tuning parameter but we can solve for the value that would lead to an approximate equilibrium between growth and mortality. Solving for

$$\frac{1}{NS}\frac{d(NS)}{dt} = 0 \tag{18}$$

after some algebra yields $m = f_s G$, and with $a = 1$ this becomes

$$\frac{m_0}{I_0} = \epsilon f_s \tag{19}$$

Averaging $f_s$ over the maturation period $0 \leq D \leq 1$ with $D_s = 0.35$ and assuming $\epsilon \approx 0.3$ gives $m_0/I_0 = 0.2$. This is the default level of predation in the model except where otherwise specified.

### 2.2.6 Activity level and diapause

Modulation of activity level $a$ has been treated as simply as possible, using a "myopic" criterion that considers only the instantaneous energy budget, rather than an optimisation over the annual routine or lifetime (Sainmont et al., 2015). Furthermore, we treat $a$ as a binary switch—diapause or full foraging activity—although intermediate overwintering states have been sometimes observed, e.g., *C. glacialis/marshallae* on the Eastern Bering Sea shelf in November (R. G. Campbell, pers. comm.), and a continuously varying $a$ could be used to represent modulations in diel vertical migration or foraging strategy more generally. In the present model, we set $a = 0$ if $D > D_{dia}$ (the stage at which diapause first becomes possible) and prey saturation $\sigma$ is below a threshhold $\sigma_{crit}$, and set $a = 1$ otherwise. The prey saturation threshhold is determined by maximising the rate of total population energy gain as a function of $a$. When $d/da$ of this quantity is positive, active foraging $a = 1$ is the optimal instantaneous strategy and when it is negative, $a = 0$ is optimal. I.e., the threshhold

$$\frac{d}{da}\frac{d}{dt}(\varphi + S)N = 0 \tag{20}$$

can be rearranged to give

$$\sigma_{crit} = \frac{r_m(1 - r_b)}{r_a} + \frac{C_{dia}}{r_a}\frac{m_0}{I_0} \tag{21}$$

where $C_{dia} = 1 + \varphi/S$. The first term in (21) can be derived more simply by setting $dG/da = 0$, a criterion based on ingestion and metabolism alone. The second term adjusts this criterion by discouraging foraging at marginal prey concentrations when predation is high. This second term, however, tends to produce

unrealistic, rapid oscillations in which the copepods briefly "top up" on prey and then hide in a brief "diapause" to burn them: this is the limitation of a myopic criterion in which diapause is not explicitly required to be seasonal, and of combining actual lipid reserves and potential egg production into a single state variable. Pragmatically, the issue can be eliminated by replacing $C_{dia}$ with 1 + $R/S$; or, to preserve the self-sufficiency of the $\varphi$ model, by approximating $C_{dia}$ as

$$C_{dia} = \max\left[0,\ \ 1 + \min\left(r_{\varphi}^{max}, \frac{\varphi}{S}\right)\right] \tag{22}$$

where $r_{\varphi}^{max} = 1.5$.

## 2.3 Population-level response

The viability of a trait combination in a given environment can be expressed in terms of the egg fitness $F$, future egg production per egg (Varpe et al., 2007). $F$ depends on spawning timing $t_0$, which we assume a copepod population is completely free to optimise: we do not impose any constraints representing environmental cues or additional physiological requirements. The approach to optimising $t_0$ and solving for $F$ differs between the $\varphi$ and ER versions of the model, which we will discuss separately. However, both methods require an estimate of individual egg biomass $W_e$ in order to convert $\varphi(t)$ or $E(t)$ from carbon units into a number of eggs, and so a digression on the determination of $W_e$ is required.

### 2.3.1 Egg and adult size

The problem of estimating $W_e$ can be replaced by the problem of estimating adult size $W_a$ using the empirical relationship for broadcast spawners determined by Kiørboe and Sabatini (1995):

$$\ln W_e \approx \ln r_{ea} + \theta_{ea} \ln W_a \tag{23}$$

where $r_{ea} = 0.013$, $\theta_{ea} = 0.62$. (In the ER model, $W_a \equiv S + R$ at $D = 1$, but in the $\varphi$ model we approximate it as $S$ alone for simplicity.) Adult size itself is an important trait for the model to predict, but the controls on it are rather buried in the model formulation above. Banas and Campbell (2016) describe a theory relating body size to the ratio of development rate to growth rate based on a review of laboratory data for copepods with adult body sizes 0.3–2000 $\mu$gC. In our notation, their model can be derived as follows: if we approximate (10), (11) in terms of a single biomass variable as

$$\frac{dW}{dt} = \epsilon'\, q_g\, I_0\, W^{\theta},\ \ D \geq D_f \tag{24}$$

then integrating from spawning to maturation gives

$$\frac{1}{1-\theta} W^{1-\theta}\Big|_{D=0}^{D=1} = (1 - D_f)\, \epsilon'\, q_g\, I_0\, \frac{1}{u} \tag{25}$$

since $u$ is the reciprocal of the total development time. Growth rate has been written in terms of $I_0$ and an effective growth efficiency over the development period $\epsilon'$. If we assume that egg biomass $W_e = W|_{D=0}$ is much smaller than $W_a = W|_{D=1}$, then combining (25) with (2) gives

$$W_a \approx \left[(1-\theta)\,(1-D_f)\ \epsilon'\ \left(\frac{Q_g}{Q_d}\right)^{T/10^{\circ}\mathrm{C}} \frac{I_0}{u_0}\right]^{\frac{1}{1-\theta}} \tag{26}$$

**Table 1.** Parameter values and other symbols used in the manuscript.

| Symbol | Definition | Value | Units | Source |
|---|---|---|---|---|
| $a$ | Activity level | | | |
| $a^\star$ | Variation of metabolism with $a$ | | | |
| $C_{dia}$ | Coefficient arising in the diapause criterion | | | |
| $D$ | Relative developmental stage | | | |
| $D_{dia}$ | Stage at which diapause becomes possible | 0.49 | | stage C3 |
| $D_f$ | Stage of first feeding | 0.1 | | stage N3; Campbell et al. (2001) |
| $D_s$ | Stage at which lipid storage begins | 0.35 | | stage C1 |
| $E$ | Total egg production | | $\mu$gC d$^{-1}$ | |
| $E_{cap}$ | Capital egg production | | $\mu$gC d$^{-1}$ | |
| $E_{inc}$ | Income egg production | | $\mu$gC d$^{-1}$ | |
| $E_{max}$ | Maximum egg production rate | | $\mu$gC d$^{-1}$ | |
| $F$ | Egg fitness | | | |
| $F_{1/2}, F_1, F_2$ | Maximum egg fitness at 1/2, 1, 2 generations per year | | | |
| $f_s$ | Fraction of $G$ allocated to $S$ | | | |
| $G$ | Net gain (ingestion minus metabolism) | | d$^{-1}$ | |
| $I$ | Specific ingestion | | d$^{-1}$ | |
| $I_0$ | Specific ingestion at $\sigma = 1$, $T = 0°$C, $S = 1$ $\mu$gC | 0.4 | d$^{-1}$ | Banas and Campbell (2016) |
| $K_s$ | Half-saturation for ingestion | See Table 2 | mg chl m$^{-3}$ | Møller et al. (????), Campbell et al. (2016) |
| $M$ | Specific metabolism | | d$^{-1}$ | |
| $m$ | Specific predation mortality | | d$^{-1}$ | |
| $m_0$ | Specific predation mortality at $T = 0°$C, $S = 1$ $\mu$gC | See Table 2 | d$^{-1}$ | |
| $N$ | Survivorship | | | |
| $P$ | Prey concentration | | mg chl m$^{-3}$ | |
| $Q_d$ | $Q_{10}$ for development | 3.0 | | Forster et al. (2011) |
| $Q_g$ | $Q_{10}$ for growth | 2.5 | | Forster et al. (2011) |
| $q_d$ | Temperature dependence of development | | | |
| $q_g$ | Temperature dependence of growth | | | |
| $R$ | Individual reserve biomass | | $\mu$gC | |
| $r_a$ | Fraction of ingestion assimilated | 0.67 | | |
| $r_b$ | Diapause metabolism relative to active metabolism | 0.25 | | Maps et al. (2014) |
| $r_{ea}$ | Scaling constant for egg:adult size ratio | 0.013 | | Kiørboe and Sabatini (1995) |
| $r_m$ | Metabolism relative to prey-saturated ingestion | 0.14 | | |
| $r_{starv}$ | Fraction of $S$ consumable under starvation conditions | | | |
| $r_\varphi^{max}$ | Upper limit on $\varphi/S$ used in diapause criterion | 1.5 | | *C. hyperboreus* lipid fraction: Swalethorp et al. (2011) |
| $S$ | Individual structural biomass | | $\mu$gC | |
| $T$ | Temperature experienced by the organism | | °C | |
| $T_0$ | Surface temperature | | °C | |
| $T_d$ | Deep temperature | | °C | |
| $t$ | Simulation time | | d | |
| $t_{egg}$ | Earliest possible date of egg production | See Table 2 | d | |
| $t_0$ | Yearday of spawning | | d | |
| $u$ | Ontogenetic development rate | | d$^{-1}$ | |
| $u_0$ | Development rate corrected to 0°C | See Table 2 | d$^{-1}$ | |
| $W_a$ | Adult body size | | $\mu$gC | |
| $W_e$ | Egg biomass | | $\mu$gC | |
| $\delta t$ | Effective duration of prey availability (global testbed) | | | |
| $\delta t'$ | Width of $P$ window (global testbed) | | | |
| $\epsilon$ | Gross growth efficiency | | | |
| $\epsilon'$ | Effective $\epsilon$ over the development period | | | |
| $\theta$ | Allometric exponent for vital rates | 0.7 | | Saiz and Calbet (2007) |
| $\theta_{ea}$ | Allometric exponent for egg:adult size ratio | 0.62 | | Kiørboe and Sabatini (1995) |
| $\lambda$ | Population growth rate | | yr$^{-1}$ | |
| $\sigma$ | Prey saturation | | | |
| $\sigma_{crit}$ | Critical prey saturation for diapause criterion | | | |
| $\varphi$ | Potential reserves and egg production | | $\mu$gC | |

Properly speaking, both $\epsilon'$ and $T$ in (26) are functions of $t_0$ since they depend on the alignment of the development period with the annual cycle. Since we are trying to use (23) and (26) to optimise $t_0$, we have a circular problem. Record et al. (2013) derive an expression similar to (26) and apply it iteratively because of this circularity. Some applications of Coltrane might require the same level of accuracy, but in the present study we take the expedient approach of simply assuming that $T$ is the annual mean of $T_0$ and that $\epsilon' \approx 1/3$: i.e., that after $t_0$ is optimised, some diapause/spawning strategy will emerge that aligns the maturation period moderately well with a period of high prey availability. This assumption eliminates the need to run the model before estimating $W_e$ via (23) and (26).

### 2.3.2 Optimal timing in the $\varphi$ model

With a method for approximating $W_e$ in hand, we can define egg fitness $F$ as a function of $\varphi$. If a cohort spawned on $t_0$ were to convert all of its accumulated free scope $\varphi$—all net energy gain beyond that required to build an adult body structure—into eggs on a single day $t_1$, the eggs produced per starting egg would be

$$F(t_0 \to t_1) = \frac{\varphi(t_1)}{W_e} N(t_1) \tag{27}$$

This expression condenses one copepod generation into a *mapping* $F$ similar to the "circle map" of Gurney et al. (1992). Once the ODE model has been run for a family of $t_0$ cases, this mapping can be used to quickly identify optimal life cycles of any length. The optimal one-generation-per-year strategy is the $t_0$ that maximizes $F_1 = F(t_0 \to t_0 + 365)$. The optimal one-generation-per-two-years strategy has $t_0$ that maximizes $F_{1/2} = F(t_0 \to t_0 + 2 \cdot 365)$. The optimal two-generation-per-year strategy has spawning dates $t_0$, $t_1$ that maximize the product $F_2 = F(t_0 \to t_1) \cdot F(t_1 \to t_0 + 365)$; and so on. A viable strategy is a combination of spawning dates and model parameters that give $F \geq 1$.

### 2.3.3 Optimal timing in the ER model

In reality, of course, copepods are not free to physically store indefinite amounts of reserves within their bodies and then instantaneously convert them into eggs when the timing is optimal. If a scheme for calculating egg production over time $E(t)$ is added to the model (and note that this scheme has not yet been specified in our discussion), then the per-generation mapping represented by $F$ takes a different form. First, we use the assumption that the environmental annual cycle repeats indefinitely to convert the time series of $EN$—egg production discounted by survivorship—from a function of days since spawning to a function of yearday. By combining time series of $EN/W_e$ from a family of cases varying $t_0$, we construct a *transition matrix* $V$ that gives eggs spawned on each yearday in generation $k+1$, given eggs per yearday in generation $k$:

$$n_{k+1} = V \cdot n_k \tag{28}$$

where $n$ is a discrete time series spanning one year (in practice we discretize the year into 5 d segments rather than yeardays per se). The first eigenvector of $V$ then gives a seasonal pattern of egg production that is stable in shape, with the corresponding eigenvalue $\lambda$ giving one plus the population growth rate per generation: $n_{k+1}(t) = V \cdot n_k(t) = \lambda \cdot n_k(t)$. A strict criterion for strategy viability would then be $\lambda \geq 1$, although this criterion is unhelpfully sensitive to predation mortality. A more robust criterion (which we use in Section 3.4 below) is to consider a strategy viable if it yields lifetime egg production above the replacement rate: if $E(t_0; t)$ and $N(t_0; t)$ are the time series of egg production and survivorship for a cohort

spawned on $t_0$, and $n(t_0)$ is a normalized annual cycle of egg production,

$$\int_0^{365} \int_0^{\infty} n(t_0) \, \frac{E(t_0;t)N(t_0;t)}{W_e} \, dt \, dt_0 \geq 1 \tag{29}$$

Thus in the ER version of the model, as in the $\varphi$ version, we have an efficient method that describes the long-term viability of a trait combination under a stable annual cycle, along with the optimal spawning timing associated with those traits in that environment; and these methods only require us to explicitly simulate one generation.

## 2.4 Assembling communities

Community-level predictions in Coltrane take the form of bounds on combinations of traits that lead to viable populations in a given environment. There are many copepod traits represented in the model that one might consider to be axes of diversity or degrees of freedom in life strategy: $u_0$, $I_0$, $\theta$, $D_s$, $K_s$, $W_e/W_a$, and even $m_0$ to the extent that predation pressure is a function of behaviour (Visser et al., 2008). Record et al. (2013) allowed five traits to vary among competitors in their copepod community model. We have taken a minimalist approach, where in the $\varphi$ model we allow only one degree of freedom: variation in $u_0$ from 0.005–0.01 $d^{-1}$. Banas and Campbell (2016) showed from a review of lab studies that $u_0$ variations appear to be the primary mode of variation in adult size among large calanoids ($W_a > 50$ $\mu$gC) including *Calanus* and *Neocalanus* spp., with slower development leading to larger adult sizes. That study also suggests that variation in $I_0$ is responsible for copepod size diversity on a broader size or taxonomic scale (e.g. between *Calanus* and small cyclopoids like *Oithona*). However, variation in $I_0$ (energy gain from foraging) probably only makes sense as part of a tradeoff with predation risk or egg survivorship (Kiørboe and Sabatini, 1995) and we have left the formulation of that tradeoff for future work. We therefore expect Coltrane 1.0 to generate analogs for large and small *Calanus* spp. ($\sim$100–1000 $\mu$gC adult size) but not analogs for *Oithona* spp. or even small calanoids like *Pseudocalanus* or *Acartia*.

Choices regarding reproductive strategy require another degree of freedom. In the $\varphi$ model, this does not require additional parameters, because the difference between, e.g., capital spawning in winter and income spawning in spring is simply a matter of the time $t$ at which $F$ is evaluated in postprocessing: each model run effectively includes all timing possibilities (eq. (27)). In the ER model, however, diversity in reproductive timing must be made explicit. In the one experiment below that uses the ER model (Section 3.4), we use the following scheme for egg production. $E(t)$ is the sum of income egg production $E_{inc}$ and capital egg production $E_{cap}$, which are 0 until maturity is reached ($D = 1$) and an additional timing threshhold has been passed ($t > t_{egg}$). Past those threshholds, they are calculated as $E_{inc} = G$ if $G > 0$ and $E_{cap} = E_{max} - E_{inc}$ if $R > 0$, where $E_{max}$ is a maximum egg production rate which we assume to be equal to the food-saturated ingestion rate $r_a \, q_g \, I_0 \, S^{\theta}$. Thus the trait $t_{egg}$ determines whether egg production begins immediately upon maturation or after some additional delay. Instead of $t_{egg}$, expressed in terms of calendar day, one could introduce the same timing freedom through a trait linked to light, an ontogenetic clock that continues past $D = 1$, or a more subtle physiological scheme. However, since we run a complete spectrum of trait values in each environmental case, it is not important to the results how the delay is formulated, provided we only compare model output, rather than actual trait values, across cases.

## 2.5 Model experiments

This study comprises three complementary experiments (Table 2). The first of these is an idealized global testbed which addresses broad *biogeographic* patterns. The second is a testbed representing the

**Table 2.** Setup of model experiments. All other parameters are as in Table 1.

| Experiment | Environmental forcing | Variable traits | $K_s$ | $m_0$ | Model |
|---|---|---|---|---|---|
| Global | Surface, deep temperatures constant; Gaussian window of prey availability | $u_0$ = 0.005 – 0.01 d$^{-1}$ | 1 mg chl m$^{-3}$ | 0.08 d$^{-1}$ | $\varphi$ |
| Bering | Family of seasonal cycles on the middle shelf: see Appendix | $u_0$ = 0.007 d$^{-1}$ | 3 | 0.08 | $\varphi$ |
| Disko | One seasonal cycle (1996–97): see Appendix | $u_0$ = 0.005 – 0.01 d$^{-1}$, $t_{egg}$ = 0 – 1095 | 1 | 0.06 | ER |

Eastern Bering Sea shelf, which addresses *time-variability* in one population in one environment. The last is a testbed representing Disko Bay, West Greenland, which addresses *trait relationships along the size spectrum* in detail. The first two are evaluated entirely in terms of the $\varphi$ model, while in the Disko Bay case we use the ER model to allow more specific comparisons with observations.

The global testbed consists of a family of idealized environments in which surface temperature $T_0$ is held constant, and prey availability is a Gaussian window of width $\delta t'$ centered on yearday 365/2:

$$P(t) = (10 \text{ mg chl m}^{-3}) \, \exp\left[ - \left( \frac{t - \frac{365}{2}}{\delta t'} \right)^2 \right] \tag{30}$$

We assume that deep, overwintering temperature $T_d = 0.4\, T_0$. The ratio 0.4 matches results of a regression between mean temperature at 0 and 1000 m in the Atlantic between 20–90°N, or 0 and 500 m in the Pacific over the same latitudes (World Ocean Atlas 2013: http://www.nodc.noaa.gov/OC5/woa13/). We compare environmental cases in terms of $T_0$ and an effective season length $\delta t = \int \sigma \, dt$, which rescales the $\delta t'$ cases in terms of the equivalent number of days of saturating prey per year.

The Bering Sea testbed considers interannual variation in temperature, ice cover, and the effect of ice cover on in-ice and pelagic phytoplankton production (Stabeno et al., 2012b; Sigler et al., 2014; Banas et al., 2016). Variation between warm, low-ice years and cold, high-ice years has previously been linked to the relative abundance of large zooplankton including *Calanus glacialis/marshallae* (Eisner et al., 2014), and we test Coltrane predictions against 8 years of *C. glacialis/marshallae* observations from the BASIS program. Seasonal cycles of $T_0$, $T_d$, and $P$ are parameterized using empirical relationships between ice and phytoplankton from Sigler et al. (2014) and a 42-year physical hindcast using BESTMAS (Bering Ecosystem Study Ice-ocean Modeling and Assimilation System: Zhang et al. (2010); Banas et al. (2016)). Details are given in the Appendix.

The Disko Bay testbed represents one seasonal cycle of temperature and phytoplankton and microzooplankton prey, based on the 1996–97 time series described by Madsen et al. (2001). We use this particular dataset not primarily as a guide to the current or future state of Disko Bay but rather as a specific circumstance in which the life-history patterns of three coexisting *Calanus* spp. (*C. finmarchicus*, *C. glacialis*, *C. hyperboreus*) were documented (Madsen et al., 2001). Details are given in Section 3.4 and the Appendix.

# 3 RESULTS

## 3.1 An example population

One case from the global experiment with $u_0$ = 0.007 d$^{-1}$, $T_0$ = 1°C, and $\delta t$ = 135 is shown in detail in Fig. 2 to illustrate the analysis method described in Section 2.3.2. In this case, out of cohorts spawned over the full first year, only those spawned in spring reached adulthood without starving (Fig. 2b, blue–green lines; non-viable cohorts not shown). The fitness function $F$ (eq. 27) declines during winter diapause and rises during the following summer when prey are available. There is no equivalent peak during the third summer, indicating that by this time cumulative predation mortality is so high that there is no net advantage to continuing to forage before spawning.

The maximum value of $F$ for most cohorts ($\star$, Fig 2c) comes at $\sim$1.5 yr into the simulation, at the peak in prey availability following maturation. This point in the annual cycle, however, does not fall within the window of spawning dates at which maturation is possible (compare year 2 in Fig. 2c with year 1 in Fig. 2b), and thus is an example of "internal life history mismatch" (Varpe et al., 2007), the common situation in which the spawning timing that maximizes egg production by the parent is not optimal for the offspring. The long-term egg fitness corresponding to stable 1-year and 2-year cycles is marked for each cohort (Fig. 2c, red, orange circles). Some but not all of the cohorts that reach maturity are able to achieve $F > 1$, egg production above the replacement rate, in these cyclical solutions (solid circles). The best one-year and two-year strategies achieve similar maximum fitness values (red vs. orange solid dots), although they require slightly different seasonal timing.

## 3.2 Global behaviour

In the global experiment, populations like that shown in Fig. 2 were run for a spectrum of $u_0$ values, across combinations of $T_0$ and $\delta t$ from -2–16°C and 0–310 d (the latter corresponding to $\delta t'$ from 0–150 d). Across these cases, at a given $u_0$, the model predicts a log-linear relationship between adult size and temperature, which is not much perturbed by variation in prey availability (Fig. 3). The slope of this relationship is equivalent to a $Q_{10}$ of 1.8–2.0, significantly steeper than the size dependence explicitly imposed by the growth/development parameterization ($Q_d/Q_g$ = 1.2; eq. 26). This suggests that not only physiological mechanisms (Forster and Hirst, 2012) but additional, emergent, ecological mechanisms are contributing. Provocatively, a similar contrast exists between laboratory measurements of temperature dependence in *C. finmarchicus* ($Q_d/Q_g$ = 1.3, Campbell et al. (2001)) and field observations of size in relation to temperature in *C. finmarchicus* and *C. helgolandicus* across the North Atlantic ($Q_{10}$ = 1.65, Wilson et al. (2015), with prosome length converted to carbon weight based on Runge et al. (2006)).

The intercept of the size-temperature relationship depends on $u_0$ (Fig. 3), with $u_0$ = 0.005–0.01 d$^{-1}$ corresponding to the range of adult size from *C. finmarchicus* to *C. hyperboreus* at the cold end of the temperature spectrum (Disko Bay, $\sim$ 0°C: Swalethorp et al. (2011)). It is not always fair, however, to associate a particular $u_0$ value with a particular species over the full range of temperatures included. As Banas and Campbell (2016) discuss further, the temperature response of an individual species is often dome-shaped, a window of habitat tolerance (Møller et al., 2012; Alcaraz et al., 2014), whereas Coltrane 1.0 uses the monotonic, power-law response observable at the community level (Forster et al., 2011)). *C. finmarchicus*, for example, is fit well by $u_0$ = 0.007 d$^{-1}$ at higher temperatures (4–12°C), whereas near 0°C in Disko Bay, it has been observed to be considerably smaller than extrapolation along the $u_0$ = 0.007 d$^{-1}$ power law would predict. Past studies have also found *C. finmarchicus* growth and ingestion to be

suppressed at low temperatures, i.e., to show a very high $Q_{10}$ compared with the community-level value (Campbell et al., 2001; Møller et al., 2012).

With this caveat on the interpretation of $u_0$, we can observe a sensible gradation in life strategy along the $u_0$ axis (Fig. 4). From $u_0$ = 0.01 d$^{-1}$ (*C. finmarchicus*-like at 0°C) to $u_0$ = 0.005 d$^{-1}$ (*C. hyperboreus*-like), the environmental window in which multi-year life cycles are viable ($F_{1/2} \geq 1$) expands dramatically. This window overlaps significantly with the window of viability for one-year life cycles ($F_1 \geq 1$; Fig. 4, black vs. gray contours). In all $u_0$ cases, there is a non-monotonic pattern in maximum fitness as a function of either temperature or prey (Fig. 4, color contours), as environments align and misalign with integer numbers of generations per year or years per generation.

The number of generations per year in the timing strategy that optimizes $F$ for each $(T_0, \delta t)$ habitat combination is shown in Fig. 5 for $u_0$ = 0.007 d$^{-1}$. This $u_0$ value corresponds in adult size to Arctic *C. glacialis* and temperate *C. marshallae* populations in the Pacific (Fig. 3), species which coexist and are nearly indistinguishable in the Bering Sea. In the lowest-prey conditions, no timing strategy is found to be viable. As prey and temperature increase, the model predicts bands proceeding monotonically from multiple years per generation to multiple generations per year. Validating these model predictions requires parameterizing places (in terms of $T_0$ and $\delta t$) in addition to parameterizing their inhabitants, and thus the meaning of either success of failure is ambiguous. Still, we can observe the following. Ice Station Sheba in the high Pacific Arctic (Fig. 1) falls in the non-viable regime (Fig. 5), consistent with the conclusion of Ashjian et al. (2003) that *Calanus* spp. are unable to complete their life cycle there. Disko Bay falls on the boundary of one- and two-year generation lengths, consistent with observations of *C. glacialis* there (Madsen et al., 2001). At Newport, Oregon, near the southern end of the range of *C. marshallae*, the model predicts multiple generations per year, consistent with observations by Peterson (1979).

### 3.3 A high-latitude habitat limit in detail: The Eastern Bering Sea

These idealized experiments (Figs. 4,5) suggest that very short productive seasons place a hard limit on the viability of *Calanus* spp., regardless of size, temperature, generation length, or match/mismatch considerations (although these factors affect where exactly the limit falls). A decade of observations in the Eastern Bering Sea provide a unique opportunity to resolve this viability limit with greater precision. This analysis takes advantage of the natural variability on the Southeastern Bering Sea shelf described by the "oscillating control hypothesis" of Hunt et al. (2002, 2011): in warm, low-ice years, the spring bloom in this region is late ($\sim$ yearday 150: Sigler et al. (2014)) and the abundance of large crustacean zooplankton including *C. glacialis/marshallae* is very low, while in colder years with greater ice cover, the pelagic spring bloom is earlier, ice algae are present in late winter, and large crustacean zooplankton are much more abundant. The task of replicating these observations serves to test the Coltrane parameterization, and situating them within a complete spectrum of temperature/ice cover cases also allows the model to provide some insight into mechanisms.

Mean surface temperature $\overline{T_0}$ was used to index annual cycles of surface and bottom temperature on the Eastern Bering Sea middle shelf (Appendix; insets in Fig. 6). Date of ice retreat $t_{ice}$ was likewise used to index phytoplankton availability over each calendar year (Appendix; insets in Fig. 6). Coltrane was run for each ($\overline{T_0}$, $t_{ice}$) combination with $u_0$ = 0.007 d$^{-1}$, thus consistent with Fig. 5 except for the more refined treatment of environmental forcing, and an adjustment to $K_s$ to match results of Bering Sea feeding experiments (Campbell et al., 2016)). The maximum egg fitness $F$ for a one-generation-per-year strategy is shown as a function of $\overline{T_0}$ and $t_{ice}$ in the main panel of Fig. 6. Coltrane predicts that one generation per year is the optimal life cycle length everywhere in this parameter space except for the cold/ice-free and

warm/high-ice-cover extremes (white contours), combinations which do not occur anywhere in a hindcast of middle-shelf conditions back to 1971 (Fig. 6, red and blue dots).

Late summer measurements of *C. glacialis/marshallae* abundance (individuals m$^{-2}$), averaged over the middle/outer shelf south of 60°N, are shown in Fig. 6 for 2003–2010 ($n$=364 over the 8 years; Eisner et al. (2014)). Both these observations and the predicted maximum $F$ from Coltrane show a dramatic contrast between the warm years of 2003–05 ($t_{ice} = 0$) and the cold years of 2007–10 ($t_{ice}$=100–130), with the transitional year 2006 harder to interpret. Eisner et al. (2014) found that there was less contrast between cold year/warm year abundance patterns on the northern middle/outer shelf, consistent with the model prediction that all hindcast years on the northern shelf fall within the "viable" habitat range for *C. glacialis/marshallae* (Fig. 6, blue dots).

The viability threshhold that the Southeastern Bering Sea appears to straddle is qualitatively similar to that in the more idealized global experiment (Figs. 5,4), primarily aligned with the phenological index (horizontal axis) rather than the temperature index (vertical axis). The threshhold in the Bering Sea experiment falls somewhat beyond the dividing line imposed in the experiment setup between early, ice-retreat-associated blooms and late, open-water blooms ($t_{ice}$ = 75: see Appendix, Sigler et al. (2014)). This gap (whose width depends on the mortality level $m_0$: not shown) indicates that some period of ice algae availability is required by *C. glacialis/mashallae* in this system, in addition to a favorable pelagic bloom timing.

### 3.4 Coexisting life strategies in detail: Disko Bay

The experiments above test the ability of Coltrane 1.0 to reproduce first-order patterns in latitude and time but do not provide sensitive tests of the model biology. A model case study in Disko Bay, where populations of three *Calanus* spp. coexist and have been described in detail (Madsen et al., 2001; Swalethorp et al., 2011), allows a closer examination of the relationships among traits within the family of viable life strategies predicted by Coltrane.

The model forcing (Fig. 7 describes a single annual cycle, starting with the 1996 spring bloom. This represents a cold, high-ice state of the system, compared with more recent years in which the spring bloom is earlier (e.g. 2008, Fig. 7, Swalethorp et al. (2011)) and the deep layer is warmed by Atlantic water intrusions (Hansen et al., 2012). This particular year was chosen because measurements of prey availability and *Calanus* response by Madsen et al. (2001) were particularly complete and coordinated. A simple attempt to correct the prey field for quality and *Calanus* preference was made by keeping only the >11 $\mu$m size fraction of phytoplankton and adding total microzooplankton, in $\mu$g C. The measured phytoplankton C:chl ratio was used to convert the sum to an equivalent chlorophyll concentration, and this time series was then slightly idealized for clarity (Fig. 7, Appendix).

Sensible results were only possible after tuning the predation mortality scale coefficient $m_0$. It is likely that our simple mortality scheme introduces some form of bias, compared with the reality in this system of predation by successive waves of visual and non-visual predators, which will be considered in a separate study. Still, a sensitivity experiment using the $\varphi$ model shows that varying $m_0$ has, as intended, a simple, uniform effect on fitness/population growth (Fig. 8) that leaves other trait relationships along the size spectrum unaffected. The $\varphi$ model predicts that copepods similar to *C. finmarchicus* in size have much greater fitness at a generation length of one year than at two years or more; that *C. hyperboreus* would be unable to complete its life cycle in one year, but is well-suited to a two-year cycle; and that *C. glacialis* falls in the size range where one- and two-year life cycles have comparable fitness value. These results are

consistent with observations (Madsen et al., 2001) and more general surveys of life strategies in the three species (Falk-Petersen et al., 2009; Daase et al., 2013).

For greater specificity, we switched from the $\varphi$ to the ER model version, running a spectrum of $t_{egg}$ cases (see section 2.4) along with a spectrum of $u_0$ cases. The ER model imposes additional constraints on the model organisms—e.g., they are no longer allowed an infinite egg production rate—and to compensate we reduced $m_0$ from 0.08 $d^{-1}$ to 0.06 $d^{-1}$. The relationship between generation length and adult size across all ($u_0$, $t_{egg}$) combinations is shown in Fig. 9. Results are consistent with the $\varphi$ model (Fig. 8): only a one-year life cycle is viable for *C. finmarchicus* in this environment, only a two-year or longer cycle is viable for *C. hyperboreus*, and *C. glacialis* again lies near the boundary where the two strategies are comparable.

The ER model predicts a time series of egg production associated with each trait combination, not just an optimal date (Section 2.3.3), and compositing these over all viable cases within 30% of the average measured adult size for each species allows us to compare modelled egg production patterns directly with observations. The model predicts that *C. finmarchicus* analogs spawn in close association with the spring bloom, that *C. hyperboreus* spawns well before the spring bloom, and that *C. glacialis* is intermediate (Fig. 10, Fig. 11a). These patterns are all in accordance with Disko Bay observations (Madsen et al., 2001; Swalethorp et al., 2011), although the absolute range is muted: Madsen et al. (2001) report *C. hyperboreus* spawning as early as February. As one would expect from these timing patterns, the model predicts a significant trend between size and the capital fraction of total egg production $E_{cap}/(E_{inc}+E_{cap})$ (Fig. 11c). Again, the pattern is qualitatively correct but muted: Coltrane predicts 80% income breeding at the size of *C. finmarchicus* (a pure income breeder in reality) and 80% capital breeding at the size of *C. hyperboreus* (a pure capital breeder in reality). More notable than the error is how much of the income/capital spectrum can apparently be reproduced as a consequence of optimal timing alone, without imposing the physiological difference between the two strategies as an independent trait (Ejsmond et al., 2015).

The model predicts (Fig. 11b) that the largest model organisms, with the longest generation lengths, enter their first diapause near the boundary between copepodite stages C4 and C5 ($D \approx 0.75$), whereas smaller organisms enter first diapause well into stage C5. Madsen et al. (2001) found that both *C. glacialis* and *C. hyperboreus* diapause as C4, C5, and adults in Disko Bay, suggesting that the model is biased toward fast maturation. The discrepancy could also be related to intraspecific variation in the real populations or non-equiproportional development in the late stages, i.e., a variable conversion scale between actual developmental stage and $D$.

Finally, the ER version of Coltrane allows an estimate of the fraction of individual carbon in the form of storage lipids $R/(R+S)$ (Fig. 11d). Averaging each model population from $D = D_{dia}$ through adulthood, weighted by survivorship $N$, yields an overall range that compares well with the species-mean wax ester fractions measured by Swalethorp et al. (2011): ∼30% for *C. finmarchicus* to ∼60% for *C. hyperboreus*. In the middle of the size spectrum, reserve fraction is highly variable across viable two-year strategies, a warning that the success of this final model prediction may be partly fortuitous. Still, taken as a whole, this experiment has yielded a striking result: that a small set of energetic and timing contraints is able to correctly predict, a priori, that Disko Bay should be able to support a spectrum of calanoid copepods from income breeders with an adult size ∼100 $\mu$g C, a one-year life cycle, and a wax ester fraction ∼30% to capital breeders with an adult size ∼1000 $\mu$g C, a two-or-more-year life cycle, and a wax ester fraction ∼60%.

# 4 DISCUSSION

## 4.1 Uncertainties

The biology in Coltrane could be refined in many ways, but two issues stand out as being both mechanistically uncertain and sensitive controls on model behaviour. These correspond to the two parameters that it was necessary to tune among model experiments (Table 2): the obstacles to formulation of a single, fully portable scheme.

The first of these is the perennial problem of the mortality closure. We modelled predation mortality as size-dependent according to the same power law used for ingestion and metabolism, a choice which is mathematically convenient and makes the effect of top-down controls, if not minor, then at least simple and easy to detect (Fig. 8). This size scaling is consistent with the review by Hirst and Kiørboe (2002) but that study also shows that the variation in copepod mortality not explained by allometry spans orders of magnitude (cf. Ohman et al. (2004)). Indeed, in some cases one might posit exactly the opposite pattern, in which mortality due to visual predators like larval fish increases with prey body size (Fiksen et al., 1998; Varpe et al., 2015). This latter pattern is one hypothesis for why in reality *C. hyperboreus* is confined to high latitudes, whereas the model predicts no southern (warm, high-prey) habitat limit to *C. hyperboreus* analogs based on bottom-up considerations (Fig. 4). Merging Coltrane 1.0 with a light- and size-based predation scheme similar to Varpe et al. (2015) or Ohman and Romagnan (2015) would allow one to better test the balance of bottom-up and top-down controls on calanoid biogeography.

Second, our experience constructing the Bering Sea and Disko Bay cases suggests that the greatest uncertainty in the model bioenergetics is actually not the physiology itself—empirical reviews like Saiz and Calbet (2007), Maps et al. (2014), Kiørboe and Hirst (2014), and Banas and Campbell (2016) have constrained the key rates moderately well—but rather the problem of translating a prey field into a rate of ingestion. Within each of our model testbeds, the prey time series $P$ remains subject to uncertainty in relative grazing rates on ice algae, large and small pelagic phytoplankton, and microzooplankton, despite a wealth of local observations and a history of work on this problem in *Calanus* specifically (Olson et al., 2006; Campbell et al., 2016). The precision of each testbed, and even moreso the ambition of generalizing across them, is also limited by uncertainty in the half-saturation coefficient, which does not appear to be consistent across site-specific studies (Campbell et al., 2016; Møller et al., ????) or well-constrained by general reviews (Hansen et al., 1997), and more generally by uncertainty in the functional form (Gentleman et al., 2003). This ambiguity is perhaps not surprising when one considers that ingestion as a function of chlorophyll or prey carbon is not a simple biomechanical property, but in fact a plastic behavioural choice. Accordingly, it might well be responsive not only to mean or maximum prey concentration but also to the prey distribution over the water column, the tradeoff between energy gain and predation risk (Visser and Fiksen, 2013), prey composition and nutritional value, and the context of the annual routine. These issues are fundamental to concretely modelling the effect of microplankton dynamics on mesozooplankton grazers. Addressing them systematically in models will require novel integration between what could be called oceanographic and marine-biological perspectives on large zooplankton.

## 4.2 Temperature and timing

Despite these uncertainties, one pattern in the copepod response to environment appears to hold in Coltrane whether prey availability is treated simply (Fig. 5,4) or with site-specific detail (Fig. 6). Namely, the viability of the calanoid community, at least near its high-latitude limit, is more sensitive to prey abundance and phenology than to temperature. Alcaraz et al. (2014) suggested based on lab experiments

that *C. glacialis* reaches an bioenergetic limit near 6°C, and Holding et al. (2013) and others have hypothesized that thermal limits will produce ecosystem-level tipping points in the warming Arctic. Our results, in contrast, suggest that thermal tipping points, even if present at the population level, do not generalize to the community level in copepods. Rather, the model predicts complete continuity between the life strategy of Arctic *C. glacialis* and temperate congeners like *C. marshallae* (Fig. 5). It also suggests that even on the population level in the Bering Sea, warm/cold-year variation in prey availability is a sufficient explanation of variability in the abundance of *C. glacialis/marshallae* (Fig. 6), without the invocation of a thermal threshhold.

Both the global and Bering experiments suggest, furthermore, that increasing water temperature per se is not necessarily a stressor on copepod communities, even high-latitude communities. In both cases, the low-prey viability threshhold actually relaxes (i.e. is tilted toward lower prey values) as temperature increases, indicating that in these testbeds, the positive effect of temperature on growth and maturation rate actually outweighs the effect of temperature on metabolic losses and overwinter survival. In cases where deep, overwintering temperatures increase faster than surface temperatures (Hansen et al., 2012) this balance may not hold, and in the real ocean changes in temperature are highly confounded with changes in phytoplankton production and phenology. Still, it is notable that the model predicts that warming temperatures will have a non-monotonic effect on copepod populations ($\partial F/\partial T_0 \gtrless 0$, Figs. 5,4) even when metabolic thermal threshholds *sensu* Alcaraz et al. (2014) and changes in prey availability are not considered. These results are a caution against overly simple climate-impacts projections based on temperature alone.

## 5 CONCLUSION

Coltrane 1.0, introduced here, is a minimalist model of copepod life history and population dynamics, a metacommunity-level framework on which additional species- or population-level constraints can be layered. Many present and future patterns in large copepods might well prove to be sensitive to species-specific constraints that Coltrane 1.0 does not resolve, such as thermal adaptation, physiological requirements for egg production, or cues for diapause entry and exit. Nevertheless, the model experiments above demonstrate that many patterns in latitude, time, and trait space can be replicated numerically even when we only consider a few key constraints on the individual energy budget: the total energy available in a given environment per year; the energy and time required to build an adult body; the metabolic and predation penalties for taking too long to reproduce; and the size and temperature dependence of the vital rates involved.

Results of the global and Bering experiments (Figs. 5,4,6) suggest that timing and seasonality are crucial to large copepods, but not because of match/mismatch (Edwards and Richardson, 2004): the model organisms are free to resolve timing mismatches with complete plasticity. Rather, these results highlight the role of seasonality in the sense of total energy available for growth and development per year, or the number of weeks per year of net energy gain relative to the number of weeks of net deficit. The simplicity of this view means that the model scheme and results may generalize far beyond copepods with only minor modification.

The exercise of parameterizing the Bering Sea and Disko Bay cases, and of attempting to map real environments onto an idealized parameter space in the global experiment (Fig. 5), highlighted that the real limit on our ability to predict the fate of copepods in changing oceans may not be our incomplete knowledge of their biology, but rather our incomplete knowledge of how their environments appear from

their point of view. How do standard oceanographic measures of chlorophyll and particulate chemistry relate to prey quality, and how much risk a copepod should take on in order to forage in the euphotic zone? How do bathymetry, the light field, and other metrics relate to the predator regime? Further experiments in a simple, fast, mechanistically transparent model like Coltrane may suggest new priorities for field observations, in addition to new approaches to regional and global modelling.

## APPENDIX: REGIONAL TESTBED FORMULATIONS

### Eastern Bering Sea

This Appendix specifies the formulation of the Bering Sea and Disko Bay testbeds in detail.

Interannual variation in the Bering Sea was parameterized for a swath of the middle shelf bounded by two long-term mooring sites on the 70 m isobath: M2 (57°N), representing the southern shelf where seasonal ice cover is highly variable and some winters are ice-free, and M8 (62°N), representing the northern shelf where seasonal ice cover is more consistent (Stabeno et al., 2012a). An annual cycle at one station is parameterized in terms of the annual mean surface temperature $\overline{T_0}$ and yearday of spring/summer ice retreat $t_{ice}$.

Annual cycles of surface and bottom temperature $T_0(t)$, $T_d(t)$ were associated with $\overline{T_0}$ using results from a 1971–2012 three-dimensional, assimilative hindcast using the BESTMAS model (Zhang et al., 2010; Banas et al., 2016). This hindcast compares well with observations of ice area and thickness, in both the mean seasonal cycle and interannual anomalies (Zhang et al., 2010). It also shows excellent agreement with the areal mean and standard deviation of surface and bottom temperatures on the shelf (Zhang et al., 2012). Fitting idealized curves to daily BESTMAS output at M2, M8, and the intermediate mooring sites M4, M5 lets us concisely represent $T_0(t)$ in terms of $\overline{T_0}$ as two half-sinusoids:

$$T_0(t) = \max(-1.8°\mathrm{C},\ \ -3.1°\mathrm{C} + 1.5\,\overline{T_0} + \Delta T \cdot \cos\left(\frac{2\pi}{365}(t - t_{max})\right)$$

$$\Delta T = \begin{cases} -0.62\,\overline{T_0} + 9.6°\mathrm{C} & ,\ |t - t_{max}| < 365/4 \\ 0.76\,\overline{T_0} + 0.2°\mathrm{C} & ,\ |t - t_{max}| \geq 365/4 \end{cases}$$

where $t_{max}$ = yearday 245. A parallel polynomial expression for $T_d(t)$ is

$$T_d(t) = \max\left[-1.8°\mathrm{C},\ \ 1.75°\mathrm{C} \cdot (\hat{t} - \hat{t}^5)\right]$$

where $\hat{t} = 2t/365 - 1$.

Banas et al. (2016) present a plankton model run with forcing from the same BESTMAS hindcast at the same stations, but that model covers the spring bloom period only, and so we have not used it here. Instead, we define a semi-idealized cycle of phytoplankton production based on observed patterns in spring and fall bloom timing and magnitude from moored chlorophyll sensors (Sigler et al., 2014). $P(t)$ is assembled as the day-by-day maximum of a Gaussian spring bloom $P_{spr}$; Gaussian autumn bloom $P_{aut}$; constant, low summer value in between the two $P_{sum}$; constant, even lower winter value $P_{win}$; and period of ice-algal

availability in late winter/early spring $P_{IA}$. These are given by

$$
\begin{aligned}
P_{win} &= 0.1, && t_{aut} < t < t_{spr} \\
P_{IA} &= \hat{P}_{IA}, && t \geq 45 \text{ and } t < t_{ice} + 10 \\
P_{spr} &= \hat{P}_{spr}\ \exp\left(-\left[(t - t_{spr})/15\right]^2\right) \\
P_{sum} &= \tfrac{1}{10}\ \hat{P}_{spr}, && t_{spr} < t < t_{aut} \\
P_{aut} &= \left(\tfrac{1}{2}\ \hat{P}_{spr}\right) \exp\left(-\left[(t - t_{aut})/15\right]^2\right)
\end{aligned}
$$

$\hat{P}_{spr}$ = 16 mg chl m$^{-3}$ (Sigler et al., 2014). Prey saturation during the ice algal production period (mid February until ice retreat: R. Gradinger, pers. comm.) has been assumed to be very high, comparable to the peak of the spring bloom: $\hat{P}_{IA} = \hat{P}_{spr}$. This is a gloss over a number of competing considerations. In reality, in the Eastern Bering Sea, ice algae comprise a much smaller integrated standing stock than the pelagic bloom (Cooper et al., 2013) and they are likely available to *Calanus* only intermittently in time. However, they are extraordinarily concentrated when they are present; they dominate the gut contents of *Calanus* during late winter (Durbin and Casas, 2014); and feeding experiments (Campbell et al., 2016) show that *Calanus* ingest them at a rate that far exceeds the functional response to pelagic phytoplankton we have otherwise assumed.

The date of the autumn bloom maximum $t_{aut}$, which Sigler et al. (2014) show to be relatively invariant, is 265. The date of the spring bloom maximum $t_{spr}$ has the nonlinear relationship with ice-retreat date $t_{ice}$ described by the "oscillating control hypothesis" (Hunt et al., 2002):

$$
t_{spr} = \begin{cases} 150 & , t_{ice} < 75 \\ t_{ice} + 10 & , t_{ice} \geq 75 \end{cases}
$$

Ice-free years are represented by $t_{ice} = 0$.

## Disko Bay

The Disko Bay testbed was constructed using observations of temperature, phytoplankton, and microzooplankton from 1996–97 as shown in Fig. 7 (Madsen et al., 2001). For ease of interpretation, we slightly idealized the forcing time series (instead of interpolating between raw observations) as follows.

Surface temperature is a piecewise linear function between $-0.7$°C on yearday 1, a late-winter minimum of $-1.8$°C on yearday 105, and a summer maximum of $3.7$°C on yearday 250. Deep temperature is set to $1$°C year-round, which matches 1996 observations but omits the arrival of warmer Atlantic deep water in spring 1997 (Hansen et al., 2012).

Prey $P$ is assumed to consist of large phytoplankton and microzooplankton. These were summed in carbon units and then converted to an equivalent chlorophyll concentration using the observed mean phytoplankton C:chl ratio. Similar to the Bering Sea testbed, it is assembled from the day-by-day maximum

of a Gaussian spring bloom, Gaussian autumn bloom, and constant summer and winter minima:

$$
\begin{aligned}
P_{win} &= 0.1, & t_{aut} < t < t_{spr} \\
P_{spr} &= \hat{P}_{spr}\ \exp\left(-\left[(t - t_{spr})/15\right]^2\right) & \\
P_{sum} &= \tfrac{1}{20}\,\hat{P}_{spr}, & t_{spr} < t < t_{aut} \\
P_{aut} &= \left(\tfrac{1}{2}\,\hat{P}_{spr}\right) \exp\left(-\left[(t - t_{aut})/30\right]^2\right) &
\end{aligned}
$$

$\hat{P}_{spr}$ = 13 mg chl m$^{-3}$, $\hat{P}_{spr}$ = 5 mg chl m$^{-3}$, $t_{spr}$ = yearday 150, and $t_{aut}$ = yearday 225. These timing parameters are not appropriate for more recent years with less ice cover (e.g., 2008, Fig. 7) but evaluating the effect of interannual variation on model copepods in Disko Bay, parallel to the Bering Sea experiment above, is left for future work.

## DISCLOSURE/CONFLICT-OF-INTEREST STATEMENT

The authors declare that the research was conducted in the absence of any commercial or financial relationships that could be construed as a potential conflict of interest.

## AUTHOR CONTRIBUTIONS

NSB designed the model, performed the analysis, and led the writing of the manuscript. EFM and TGN helped formulate and interpret the Disko Bay case study, and LBE the Bering Sea case study. All authors contributed to revision of the manuscript.

## ACKNOWLEDGMENTS

Many thanks to Bob Campbell, Thomas Kiørboe, Øystein Varpe, and Dougie Speirs for discussions that helped shape both the model and the questions we asked of it.

*Funding*: This work was supported by grants PLR-1417365 and PLR-1417224 from the National Science Foundation.

## REFERENCES

Alcaraz, M., Felipe, J., Grote, U., Arashkevich, E., and Nikishina, A. (2014). Life in a warming ocean: thermal thresholds and metabolic balance of arctic zooplankton. *Journal of Plankton Research* 36, 3–10

Ashjian, C. J., Campbell, R. G., Welch, H. E., Butler, M., and Van Keuren, D. (2003). Annual cycle in abundance, distribution, and size in relation to hydrography of important copepod species in the western Arctic Ocean. *Deep Sea Research Part I: Oceanographic Research Papers* 50, 1235–1261

Banas, N. S. and Campbell, R. G. (2016). Traits controlling body size in copepods: Separating general constraints from species-specific strategies. *Marine Ecology Progress Series* , subm

Banas, N. S., Zhang, J., Campbell, R. G., Sambrotto, R. N., Lomas, M. W., Sherr, E., et al. (2016). Spring plankton dynamics in the Eastern Bering Sea, 1971-2050: Mechanisms of interannual variability diagnosed with a numerical model. *Journal of Geophysical Research: Oceans* 121, 1476–1501

Beaugrand, G. and Kirby, R. R. (2010). Climate, plankton and cod. *Global Change Biology* 16, 1268–1280

Burke, B. J., Peterson, W., Beckman, B. R., Morgan, C., Daly, E. A., and Litz, M. (2013). Multivariate Models of Adult Pacific Salmon Returns. *PloS one* 8, e54134

Campbell, R. G., Ashjian, C. J., Sherr, E. B., Sherr, B. F., Lomas, M. W., Ross, C., et al. (2016). Mesozooplankton grazing during spring sea-ice conditions in the eastern Bering Sea. *Deep Sea Research Part II* in press

Campbell, R. G., Wagner, M. M., Teegarden, G. J., Boudreau, C. A., and Durbin, E. G. (2001). Growth and development rates of the copepod Calanus finmarchicus reared in the laboratory. *Marine Ecology Progress Series* 221, 161–183

Cooper, L. W., Sexson, M. G., Grebmeier, J. M., Gradinger, R., Mordy, C. W., and Lovvorn, J. R. (2013). Linkages between sea-ice coverage, pelagic-benthic coupling, and the distribution of spectacled eiders: Observations in March 2008, 2009 and 2010, northern Bering Sea. *Deep Sea Research* 94, 31–43

Coyle, K. O., Eisner, L. B., Mueter, F. J., Pinchuk, A. I., Janout, M. A., Cieciel, K. D., et al. (2011). Climate change in the southeastern Bering Sea: impacts on pollock stocks and implications for the oscillating control hypothesis. *Fisheries Oceanography* 20, 139–156

Daase, M., Falk-Petersen, S., Varpe, Ø., Darnis, G., Søreide, J. E., Wold, A., et al. (2013). Timing of reproductive events in the marine copepod Calanus glacialis: a pan-Arctic perspective. *Canadian Journal of Fisheries and Aquatic Sciences* 70, 871–884

Durbin, E. G. and Casas, M. C. (2014). Early reproduction by Calanus glacialis in the Northern Bering Sea: the role of ice algae as revealed by molecular analysis. *Journal of Plankton Research* 36, 523–541

Edwards, M. and Richardson, A. J. (2004). Impact of climate change on marine pelagic phenology and trophic mismatch. *Nature* 430, 881–884

Eisner, L. B., Napp, J. M., Mier, K. L., Pinchuk, A. I., and Andrews, A. G. (2014). Climate-mediated changes in zooplankton community structure for the eastern Bering Sea. *Deep Sea Research Part II* 109, 157–171

Ejsmond, M. J., Varpe, Ø., Czarnoleski, M., and Kozłowski, J. (2015). Seasonality in Offspring Value and Trade-Offs with Growth Explain Capital Breeding. *American naturalist* 186, E111–E125

Falk-Petersen, S., Mayzaud, P., Kattner, G., and Sargent, J. R. (2009). Lipids and life strategy of Arctic Calanus. *Marine Biology Research* 5, 18–39

Fiksen, Ø. and Carlotti, F. (1998). A model of optimal life history and diel vertical migration in Calanus finmarchicus. *Sarsia* 83, 129–147

Fiksen, Ø., Utne, A. C. W., Aksnes, D. L., Eiane, K., Helvik, J. V., and Sundby, S. (1998). Modelling the influence of light, turbulence and ontogeny on ingestion rates in larval cod and herring. *Fisheries Oceanography* 7, 355–363

Follows, M. J., Dutkiewicz, S., Grant, S., and Chisholm, S. W. (2007). Emergent biogeography of microbial communities in a model ocean. *Science* 315, 1843–1846

Forster, J. and Hirst, A. G. (2012). The temperature-size rule emerges from ontogenetic differences between growth and development rates. *Functional Ecology* 26, 483–492

Forster, J., Hirst, A. G., and Woodward, G. (2011). Growth and development rates have different thermal responses. *The American Naturalist* 178, 668–678

Gentleman, W., Leising, A. W., Frost, B. W., Strom, S. L., and Murray, J. (2003). Functional responses for zooplankton feeding on multiple resources: a review of assumptions and biological dynamics. *Deep Sea Research Part II* 50, 2847–2875

Gurney, W. S. C., Crowley, P. H., and Nisbet, R. M. (1992). Locking life-cycles onto seasons: Circle-map models of population dynamics and local adaptation. *Journal of Mathematical Biology* 30, 251–279

Hansen, J., Bjornsen, P. K., and Hansen, B. W. (1997). Zooplankton grazing and growth: Scaling within the 2-2,000 $\mu$m body size range. *Limnol Oceanogr* 42, 687–704

Hansen, M. O., Nielsen, T. G., Stedmon, C. A., and Munk, P. (2012). Oceanographic regime shift during 1997 in Disko Bay, Western Greenland. *Limnology and Oceanography* 57, 634–644

Hirche, H.-J. and Kattner, G. (1993). Egg production and lipid content of Calanus glacialis in spring: indication of a food-dependent and food-independent reproductive mode. *Marine Biology* 117, 615–622

Hirst, A. G. and Kiørboe, T. (2002). Mortality of marine planktonic copepods: global rates and patterns. *Marine Ecology Progress Series* 230, 195–209

Holding, J. M., Duarte, C. M., and Arrieta, J. M. (2013). Experimentally determined temperature thresholds for Arctic plankton community metabolism. *Biogeosciences* 10, 357–370

Hooff, R. C. and Peterson, W. (2006). Copepod biodiversity as an indicator of changes in ocean and climate conditions of the northern California current ecosystem. *Limnology and Oceanography* 51, 2607–2620

Houston, A. I., McNamara, J. M., and Hutchinson, J. M. C. (1993). General Results concerning the Trade-Off between Gaining Energy and Avoiding Predation. *Philosophical Transactions of the Royal Society of London. Series B: Biological Sciences* 341, 375–397

Hunt, G. L., Coyle, K. O., Eisner, L. B., Farley, E. V., Heintz, R. A., Mueter, F. J., et al. (2011). Climate impacts on eastern Bering Sea foodwebs: a synthesis of new data and an assessment of the Oscillating Control Hypothesis. *ICES Journal of Marine Science* 68, 1230–1243

Hunt, G. L., Stabeno, P. J., Walters, G., Sinclair, E., Brodeur, R. D., Napp, J. M., et al. (2002). Climate change and control of the southeastern Bering Sea pelagic ecosystem. *Deep Sea Research* 49, 5821–5853

Kattner, G. and Hagen, W. (2009). Lipids in marine copepods: latitudinal characteristics and perspective to global warming. In *Lipids in Aquatic Ecosystems*, ed. M. T. Arts (New York, NY: Springer New York). 257–280

Kiørboe, T. and Hirst, A. G. (2014). Shifts in Mass Scaling of Respiration, Feeding, and Growth Rates across Life-Form Transitions in Marine Pelagic Organisms. *The American Naturalist* 183, E118–E130

Kiørboe, T. and Sabatini, M. (1995). Scaling of fecundity, growth and development in marine planktonic copepods. *Marine Ecology Progress Series* 120, 285–298

Kleiber, M. (1932). Body size and metabolism. *Hilgardia* 6, 315–353

MacDonald, A., Heath, M., Edwards, M., Furness, R., Pinnegar, J., Wanless, S., et al. (2015). Climate--Driven Trophic Cascades Affecting Seabirds around the British Isles. In *Oceanography and Marine Biology* (CRC Press). 55–80

Madsen, S. D., Hansen, B. W., and Nielsen, T. G. (2001). Annual population development and production by Calanus finmarchicus, C. glacialis and C. hyperboreus in Disko Bay, western Greenland. *Marine Biology* 139, 75–83

Mantua, N. J., Hare, S. R., Zhang, Y., Wallace, J. M., and Francis, R. C. (1997). A Pacific interdecadal climate oscillation with impacts on salmon production. *Bulletin of the American Meteorological Society* 78, 1069–1079

Maps, F., Pershing, A. J., and Record, N. R. (2012). A generalized approach for simulating growth and development in diverse marine copepod species. *ICES Journal of Marine Science* 69, 370–379

Maps, F., Record, N. R., and Pershing, A. J. (2014). A metabolic approach to dormancy in pelagic copepods helps explaining inter- and intra-specific variability in life-history strategies. *Journal of Plankton Research* 36, 18–30

McNamara, J. M. and Houston, A. I. (2008). Optimal annual routines: behaviour in the context of physiology and ecology. *Philosophical Transactions of the Royal Society of London. Series B: Biological Sciences* 363, 301–319

Møller, E. F., Bohr, M., Kjellerup, S., Maar, M., Mohl, M., Swalethorp, R., et al. (????). Calanus finmarchicus egg production at its northern border . *Journal of Plankton Research*

Møller, E. F., Maar, M., Jónasdóttir, S. H., Gissel Nielsen, T., and Tönnesson, K. (2012). The effect of changes in temperature and food on the development of Calanus finmarchicus and Calanus helgolandicus populations. *Limnology and Oceanography* 57, 211–220

Ohman, M. D., Eiane, K., Durbin, E., Runge, J., and Hirche, H.-J. (2004). A comparative study of Calanus finmarchicus mortality patterns at five localities in the North Atlantic. *ICES Journal of Marine Science* 61, 687–697

Ohman, M. D. and Romagnan, J.-B. (2015). Nonlinear effects of body size and optical attenuation on Diel Vertical Migration by zooplankton. *Limnology and Oceanography* 61, 765–770

Olson, M. B., Lessard, E. J., and Wong, C. (2006). Copepod feeding selectivity on microplankton, including the toxigenic diatoms Pseudo-nitzschia spp., in the coastal Pacific Northwest. *Marine Ecology Progress Series* 326, 207–220

Österblom, H., Olsson, O., Blenckner, T., and Furness, R. W. (2008). Junk-food in marine ecosystems. *Oikos* 117, 967–977

Peterson, W. T. (1979). *Life History and Ecology of Calanus marshallae Frost in the Oregon upwelling zone*. Ph.D. thesis, Oregon State University

Record, N. R., Pershing, A. J., and Maps, F. (2013). Emergent copepod communities in an adaptive trait-structured model. *Ecological Modelling* 260, 11–24

Runge, J. A., Plourde, S., Joly, P., Niehoff, B., and Durbin, E. (2006). Characteristics of egg production of the planktonic copepod, Calanus finmarchicus, on Georges Bank: 1994–1999. *Deep Sea Research Part II* 53, 2618–2631

Sainmont, J., Andersen, K. H., Thygesen, U. H., Fiksen, Ø., and Visser, A. W. (2015). An effective algorithm for approximating adaptive behavior in seasonal environments. *Ecological Modelling* 311, 20–30

Saiz, E. and Calbet, A. (2007). Scaling of feeding in marine calanoid copepods. *Limnology and Oceanography* 52, 668–675

Sigler, M. F., Stabeno, P. J., Eisner, L. B., Napp, J. M., and Mueter, F. J. (2014). Spring and fall phytoplankton blooms in a productive subarctic ecosystem, the eastern Bering Sea, during 1995–2011. *Deep Sea Research Part II* 109, 71–83

Stabeno, P. J., Farley Jr, E. V., Kachel, N. B., Moore, S., Mordy, C. W., Napp, J. M., et al. (2012a). A comparison of the physics of the northern and southern shelves of the eastern Bering Sea and some implications for the ecosystem. *Deep Sea Research Part II* 65-70, 14–30

Stabeno, P. J., Kachel, N. B., Moore, S., Napp, J. M., Sigler, M. F., Yamaguchi, A., et al. (2012b). Comparison of warm and cold years on the southeastern Bering Sea shelf and some implications for the ecosystem. *Deep Sea Research Part II* 65-70, 31–45

Swalethorp, R., Kjellerup, S., Dünweber, M., Nielsen, T. G., Møller, E. F., Rysgaard, S., et al. (2011). Grazing, egg production, and biochemical evidence of differences in the life strategies of Calanus finmarchicus, C. glacialis and C. hyperboreus in Disko Bay, western Greenland. *Marine Ecology Progress Series* 429, 125–144

Varpe, Ø., Daase, M., and Kristiansen, T. (2015). A fish-eye view on the new Arctic lightscape. *ICES Journal of Marine Science* 72, 2532–2538

Varpe, Ø., Jørgensen, C., Tarling, G. A., and Fiksen, Ø. (2007). Early is better: seasonal egg fitness and timing of reproduction in a zooplankton life-history model. *Oikos* 116, 1331–1342

Varpe, Ø., Jørgensen, C., Tarling, G. A., and Fiksen, Ø. (2009). The adaptive value of energy storage and capital breeding in seasonal environments. *Oikos* 118, 363–370

Visser, A. W. and Fiksen, Ø. (2013). Optimal foraging in marine ecosystem models: selectivity, profitability and switching. *Marine Ecology Progress Series* 473, 91–101

Visser, A. W., Mariani, P., and Pigolotti, S. (2008). Swimming in turbulence: zooplankton fitness in terms of foraging efficiency and predation risk. *Journal of Plankton Research* 31, 121–133

Wilson, R. J., Speirs, D. C., and Heath, M. R. (2015). On the surprising lack of differences between two congeneric calanoid copepod species, Calanus finmarchicus and C. helgolandicus. *Progress in Oceanography* 134, 413–431

Zhang, J., Woodgate, R., and Mangiameli, S. (2012). Towards seasonal prediction of the distribution and extent of cold bottom waters on the Bering Sea shelf. *Deep Sea Research Part II* 65-70, 58–71

Zhang, J., Woodgate, R., and Moritz, R. (2010). Sea Ice Response to Atmospheric and Oceanic Forcing in the Bering Sea. *Journal of Physical Oceanography* 40, 1729–1747

## FIGURES

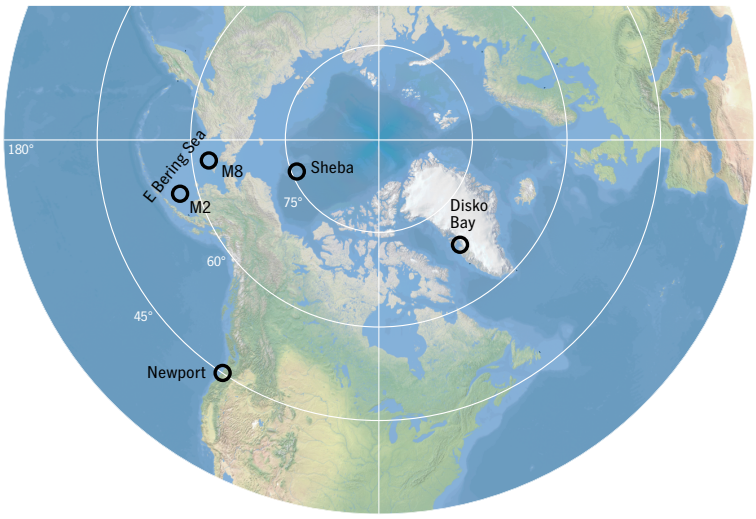


**Figure 1.** Locations of model testbeds. The "global" model experiment spans a gradient from approximately Ice Station Sheba to Newport, Oregon and beyond.

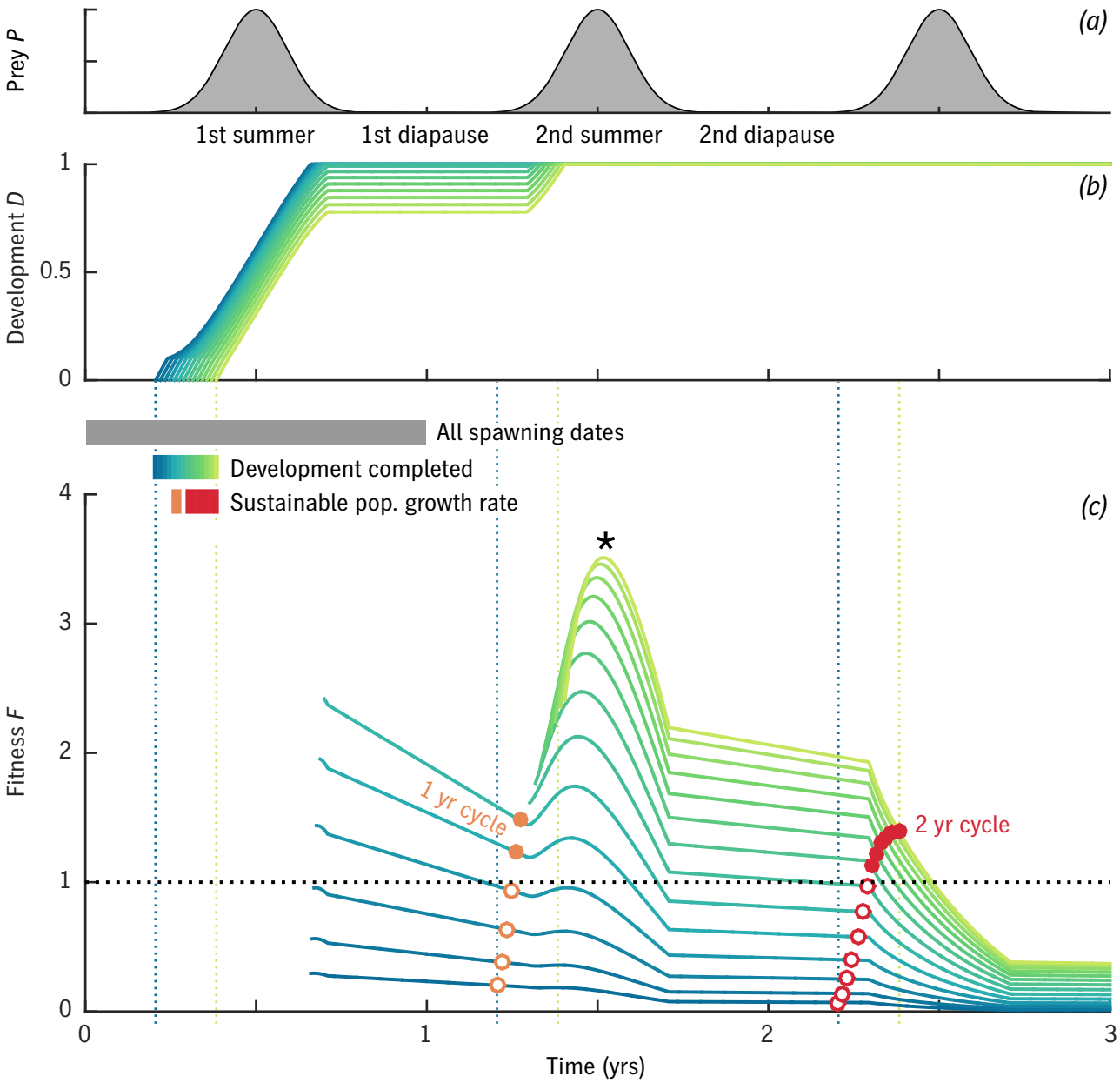


**Figure 2.** Results of an example model case with $u_0 = 0.007\ \mathrm{d}^{-1}$, $T_0 = 1°\mathrm{C}$, and $\delta t = 135$.

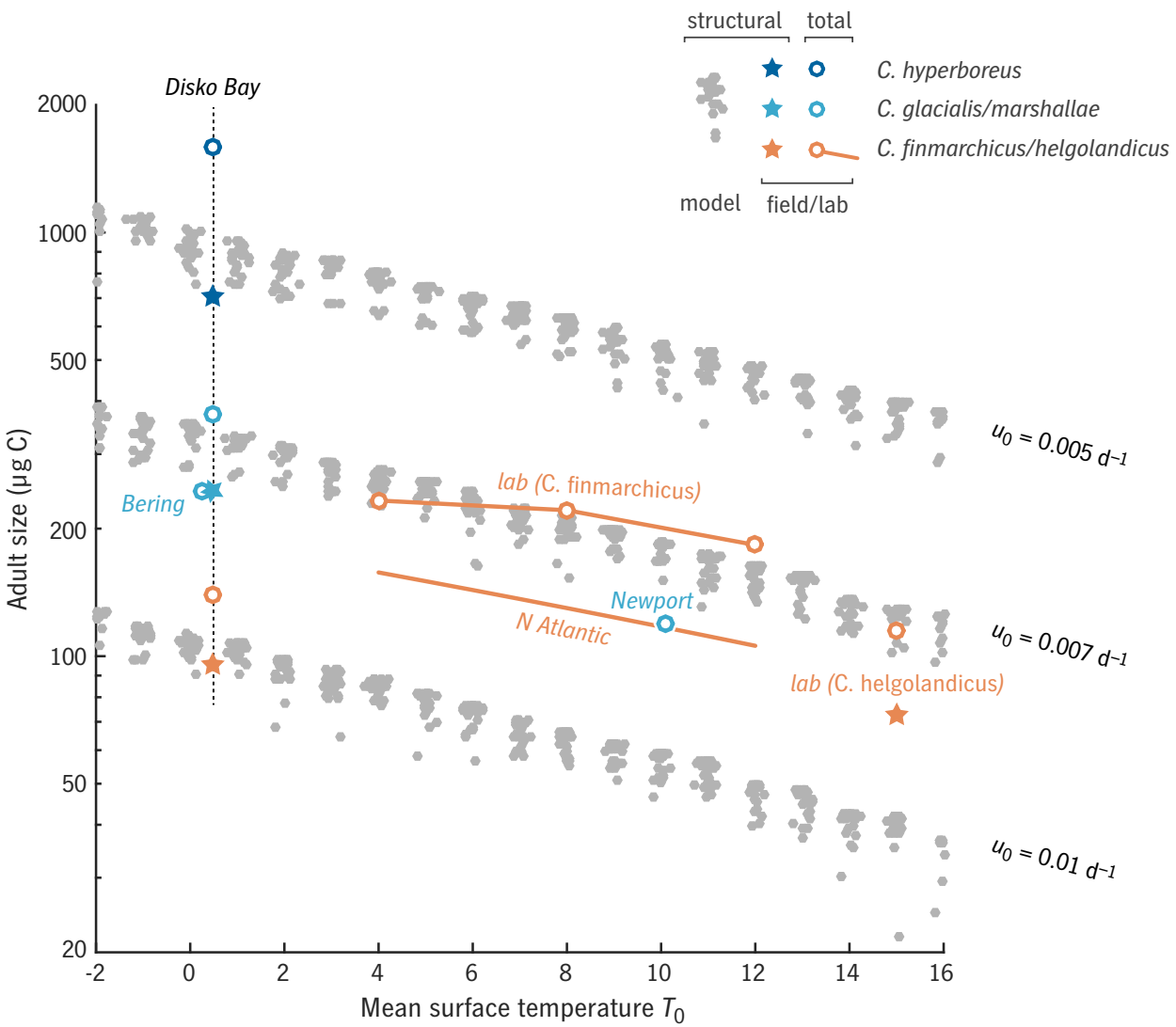


**Figure 3.** Relationship between adult size $W_a$ and mean temperature $T_0$ in the "global" model experiment, for three values of $u_0$, in comparison with observations and laboratory results. Model results (gray dots) represent structural biomass $S$, as do observations marked with a $\star$; observations marked with a $\circ$ represent total biomass $R + S$.

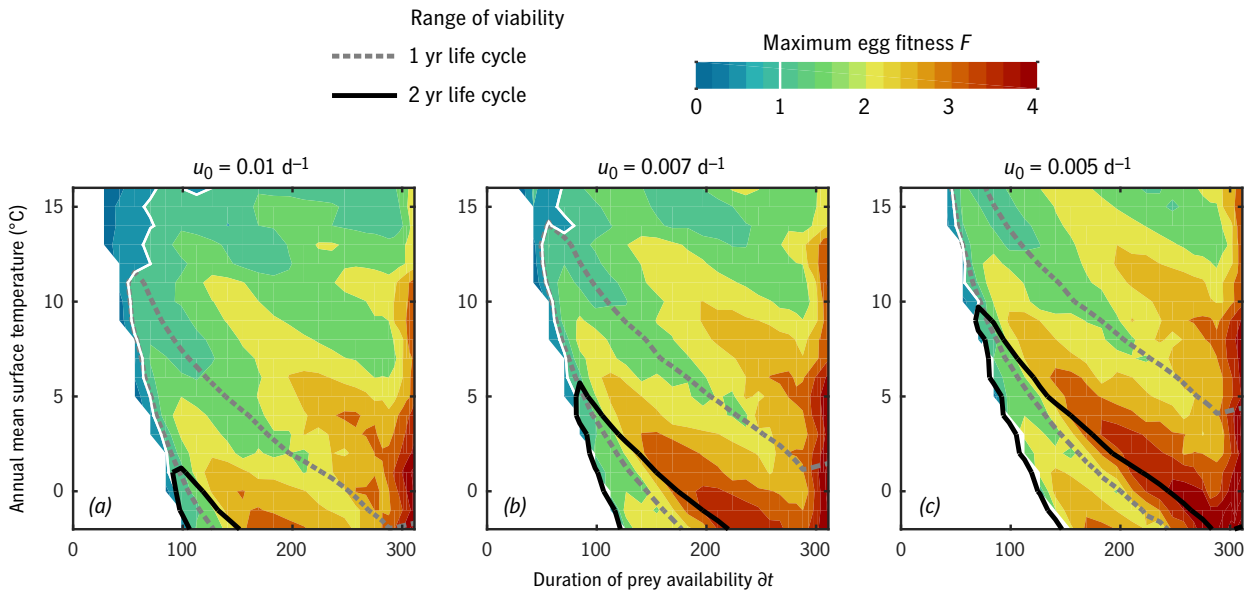


**Figure 4.** Maximum egg fitness (eggs per starting egg per generation) across all combinations of temperature and duration of prey availability in the "global" experiment. Unfilled contour lines give the environmental range over which one-year (gray, dotted) and two-year (black, solid) life cycles are viable. The white regions at low prey availability indicate environments in which no timing strategy exists that allows successful maturation.

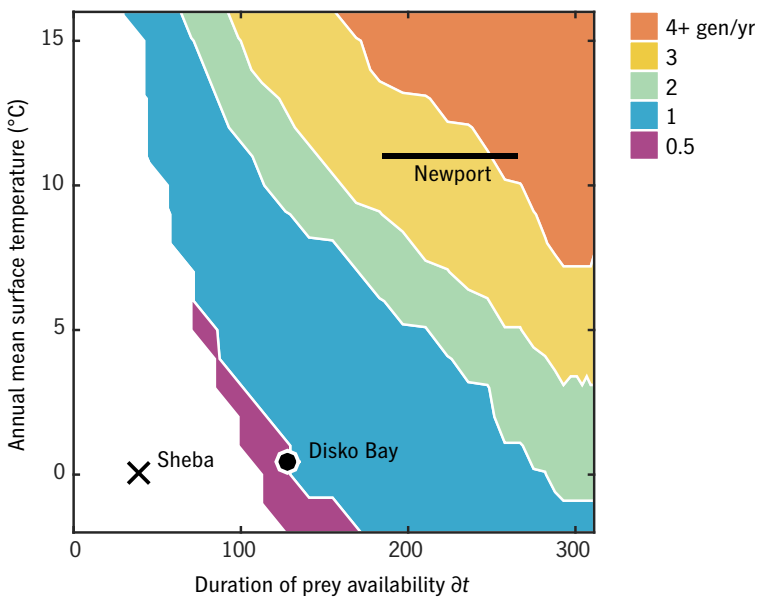


**Figure 5.** Generations per year of the optimal strategy in each environmental combination for $u_0 = 0.007$ $d^{-1}$. Ice Station Sheba, Disko Bay, and Newport (Fig. 1) have been placed approximately for comparison.

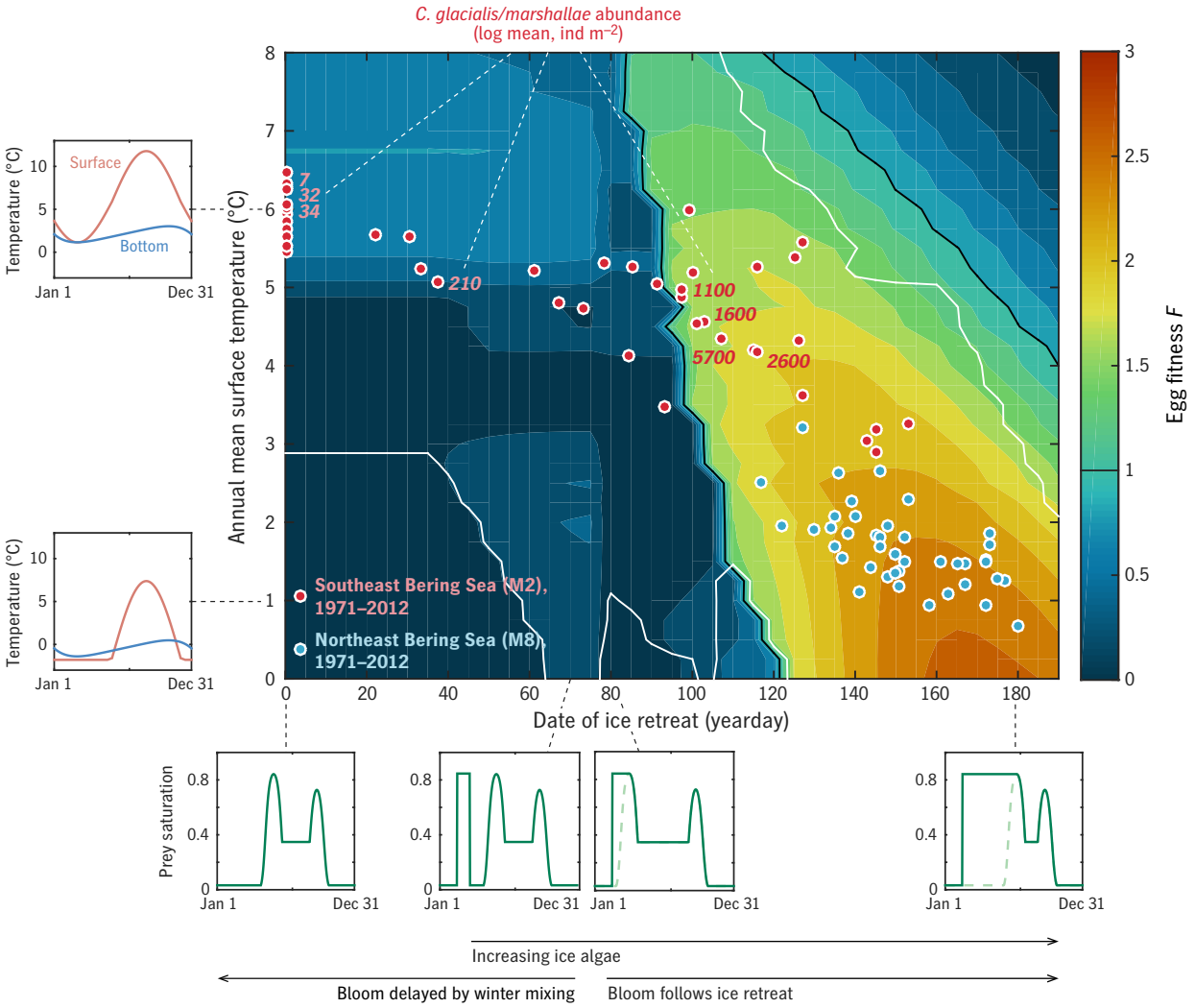


**Figure 6.** Results of the "Bering" experiment. Color contours give the predicted egg fitness of a *C. glacialis/marshallae* analog under combinations of ice retreat timing (assumed to control spring bloom timing: Appendix) and temperature. Examples of the annual cycles of prey availability $P$ and surface and bottom temperature $T_0, T_d$ are given at left and bottom. Dots locate years 1971–2012 in this timing/temperature parameter space, for the northern (blue) and southern (red) middle shelf. Numbers give the measured abundance of *C. glacialis/marshallae* in summer.

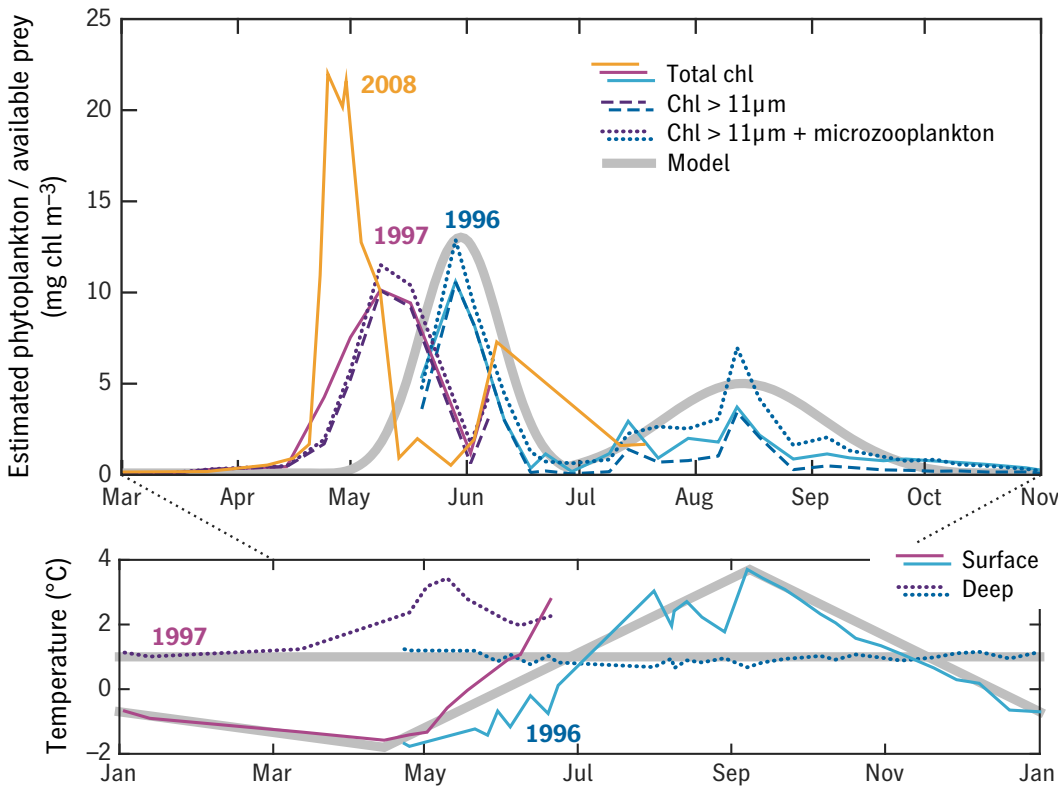


**Figure 7.** Observations of temperature and prey in Disko Bay 1996–97 from Madsen et al. (2001) (blue and purple thin lines) used to construct semi-idealized forcing time series for the model (thick grey lines). Three estimates of the prey field are shown, in each case averaged between the surface and subsurface fluorescence maximum: total chlorophyll (solid), chlorophyll in the $>11$ $\mu$m size fraction (dashed), and $>11$ $\mu$m chlorophyll plus a correction for microzooplankton (dotted). A 2008 phytoplankton time series is shown for comparison (orange), based on integrated phytoplankton carbon scaled to matched the spring maximum in chlorophyll units. Temperature in the upper 50 m ("surface") and water-column minimum temperature ("deep") are also shown.

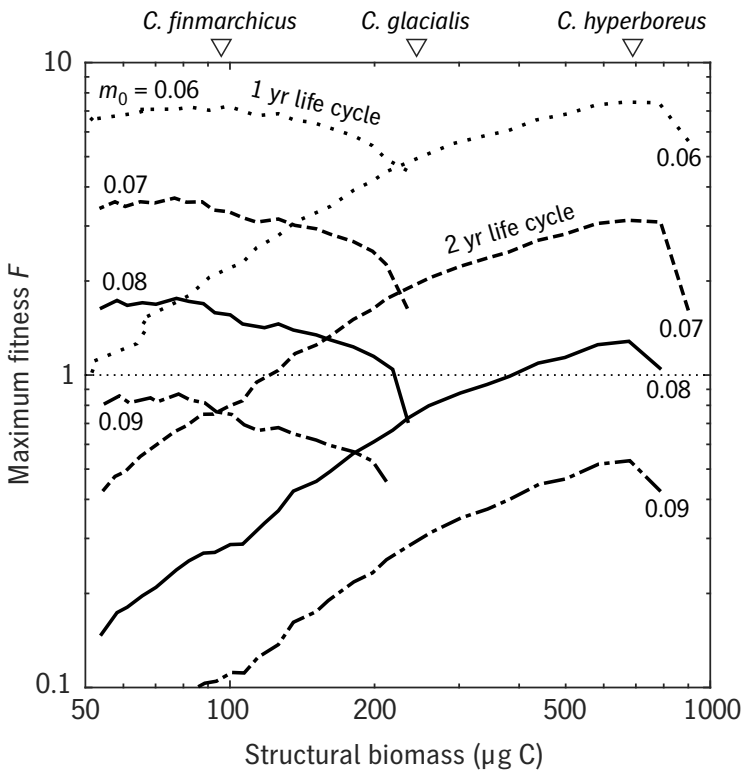


**Figure 8.** Results of the $\varphi$ model for a range of $u_0$ values in the Disko Bay testbed (Fig. 7). Maximum egg fitness $F$ is plotted for one-year and two-year strategies, for each of four values of the mortality scaling parameter $m_0$ (0.06–0.09 $d^{-1}$), as a function of adult size $S$. The mean structural weights of the three *Calanus* spp. that coexist in Disko Bay are also shown (white triangles, top). Curves of $F$ are shown over ranges where survival to adulthood without starvation is possible.

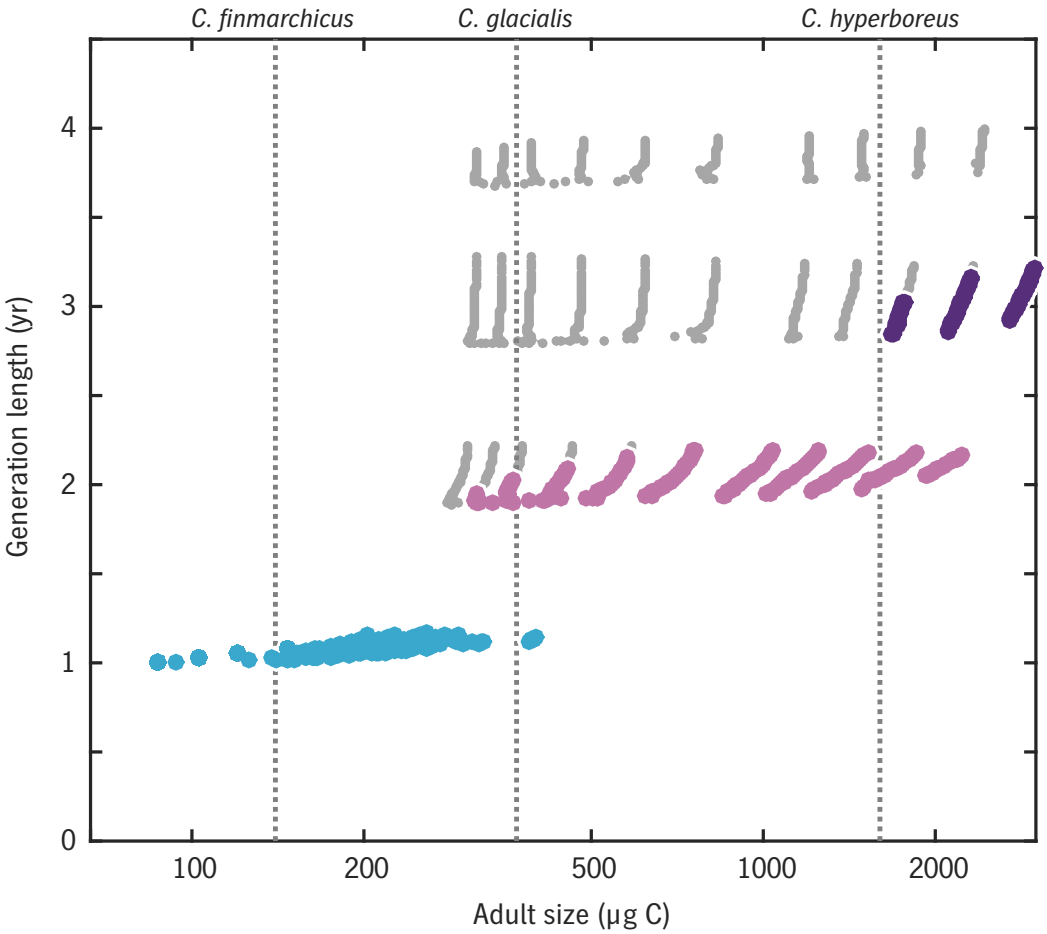


**Figure 9.** Emergent relationship between generation length and adult size in the Disko Bay model experiment. Large colored dots indicate results for trait combinations that achieve a viable rate of egg production per generation (color coding matches that in Fig. 11) while small gray dots indicate trait combinations that reach maturity without starvation but have egg production rates below replacement level.

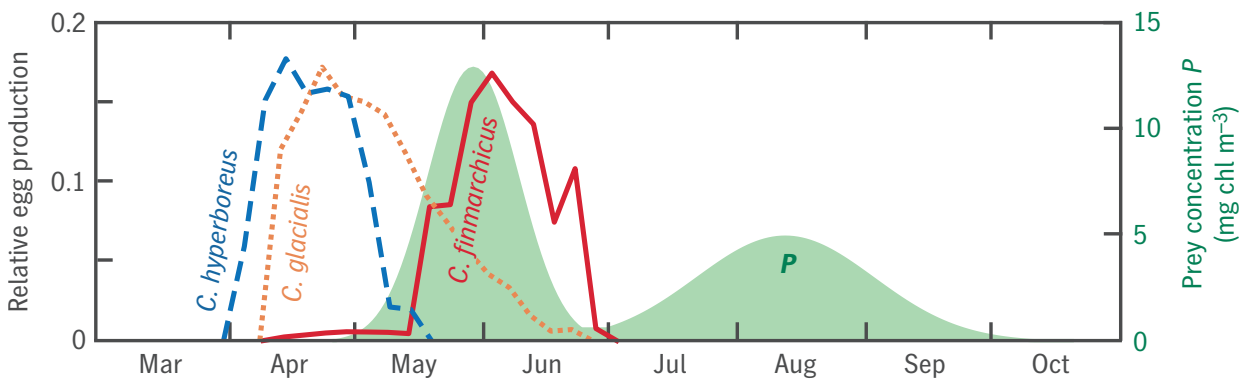


**Figure 10.** Seasonal progression of egg production in model analogs for three *Calanus* spp. in Disko Bay (lines), in relation to prey concentration $P$ (shaded). Egg production time series consist of $n(t_0)$, the first eigenvector of the transition matrix $V$ discussed in Sec. 2.3.3, normalized to integrate to 1.

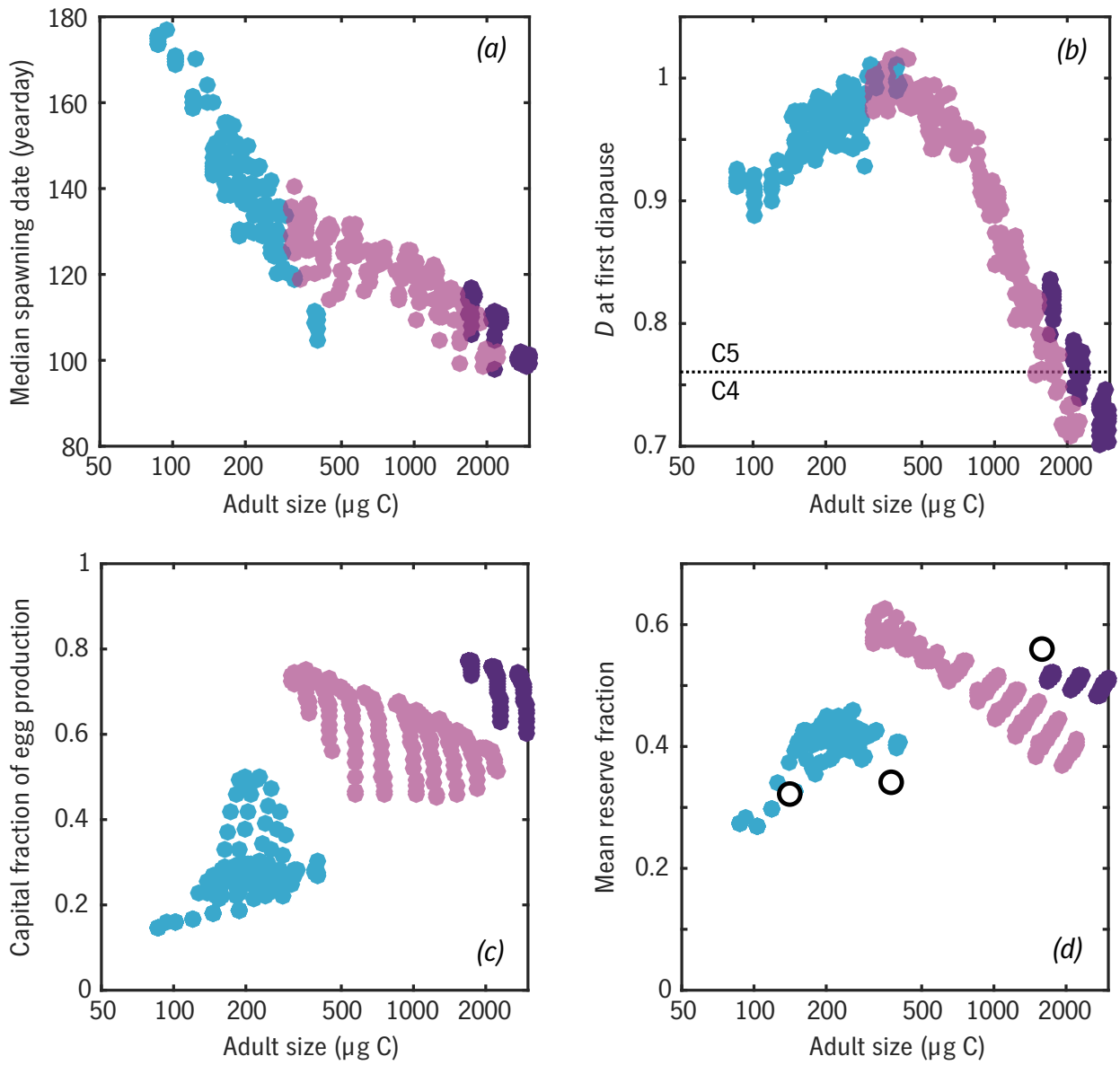


**Figure 11.** Relationships between a number of emergent traits with adult body size in the Disko Bay experiment. Color coding matches Fig. 9, distinguishing one-year (blue), two-year (light purple) and three-year (dark purple) life cycles. *(a)* Median spawning date: compare peaks of egg production curves in Fig. 10. *(b)* Earliest developmental stage $D$ at which diapause ($a = 0$) occurs: values have been jittered slightly in the vertical for clarity. *(c)* Capital fraction of egg production $E_{cap}/(E_{inc} + Ecap)$. *(d)* Mean reserve fraction of individual biomass $R/(R + S)$, compared with wax esters as a fration of total body carbon for three *Calanus* spp. from Swalethorp et al. (2011) (open circles).